The Dynamic Magnetotail: Substorms

Auroral substorm (Akasofu, 1964,
term owed to S. Chapman)

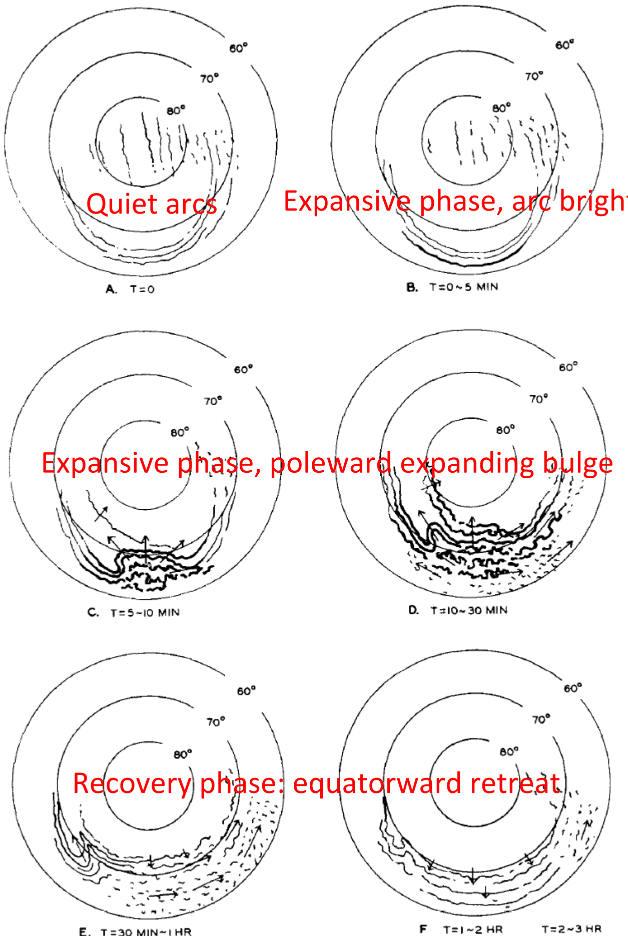

Magnetospheric substorm model
(Hones, 1977,1980)

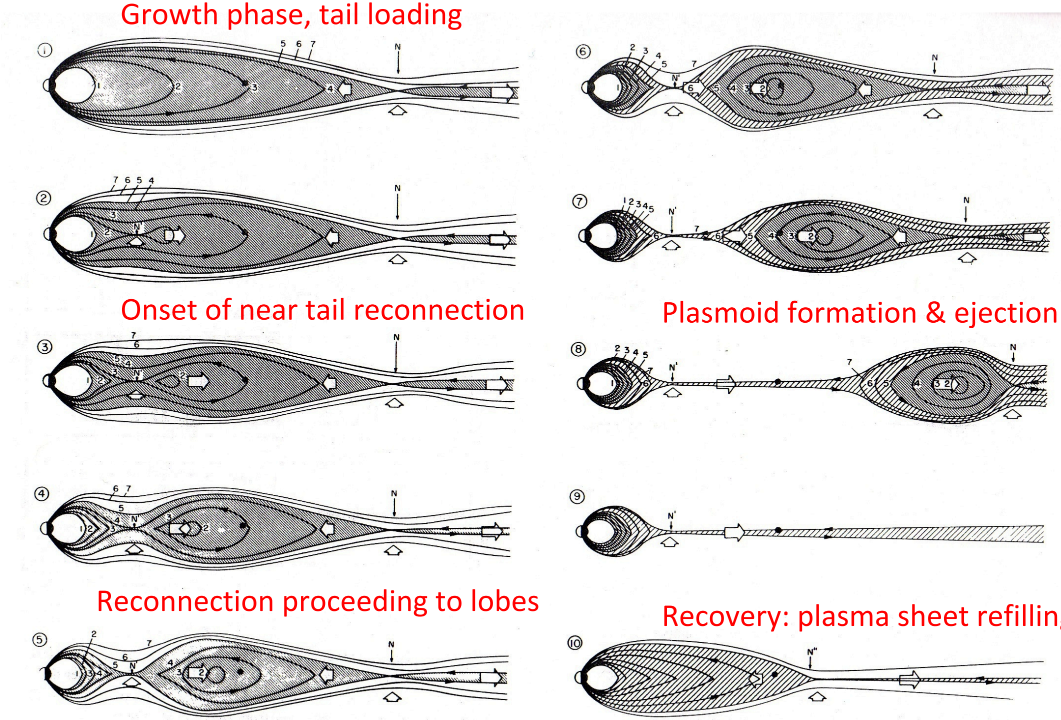

This presentation is being recorded.

The Dynamic Magnetotail: Outline

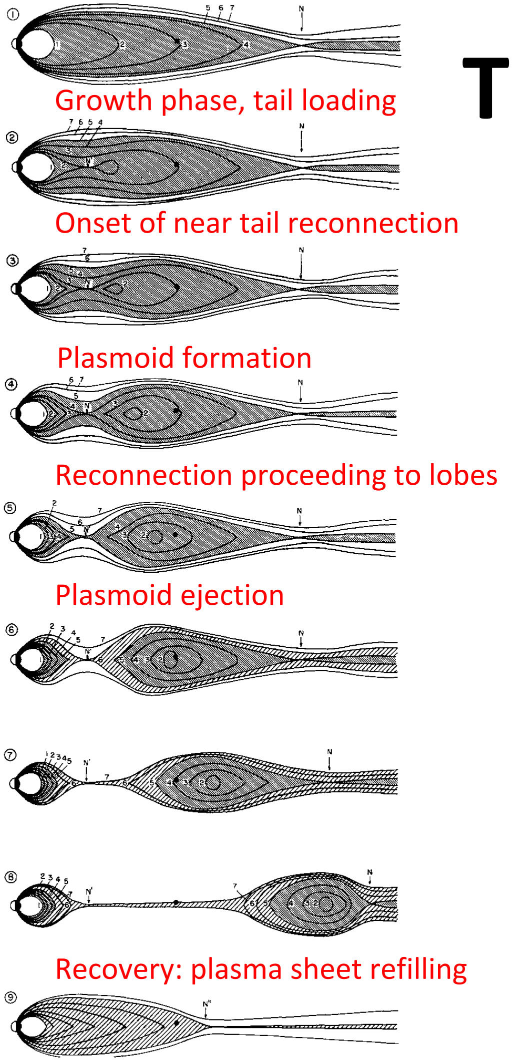

Substorm model (Hones, 1977)

1. Origin of NENL-line model
2. Formation of thin current sheet (MHD)
3. Onset of reconnection (PIC simulations)
4. Substorm Expansion (MHD simulation):

   flow bursts, dipolarization,

   substorm current wedge
5. Particle acceleration (test particles)
6. Open problems

Coppi, Laval & Pellat, 1966

Ness 1965

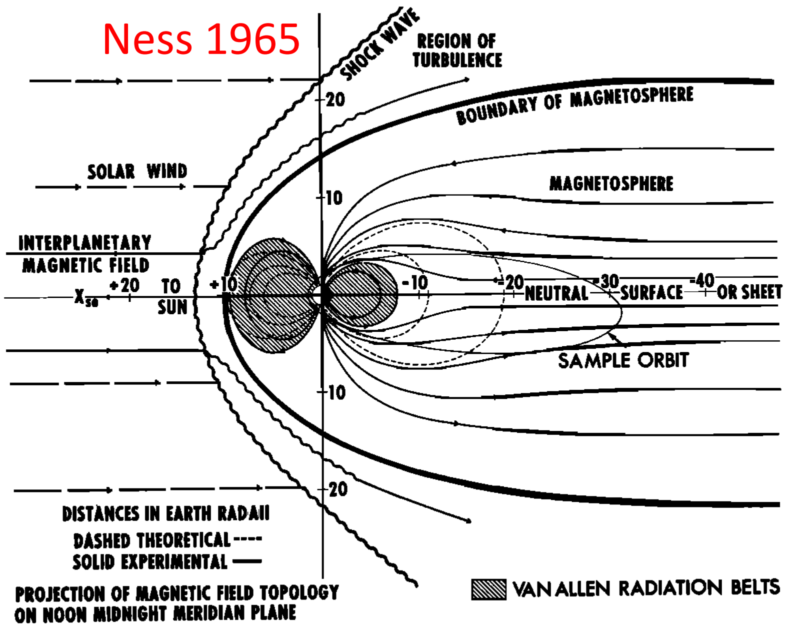

Furth+, 1963,1964

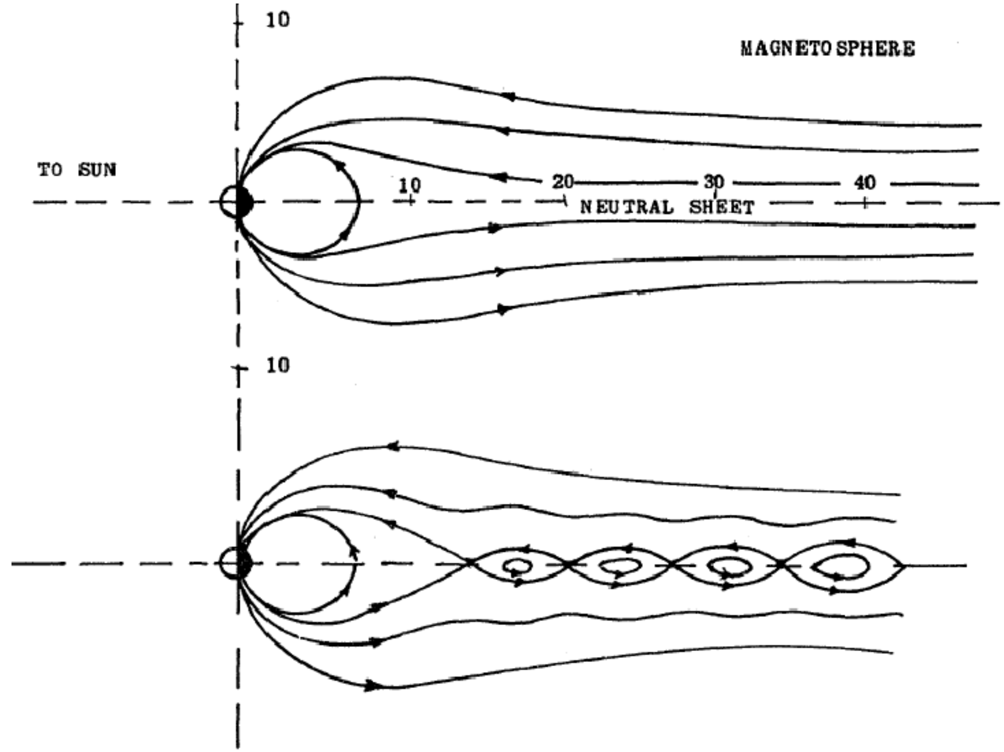

Onset of (electron) tearing mode

Atkinson 1966, 1967

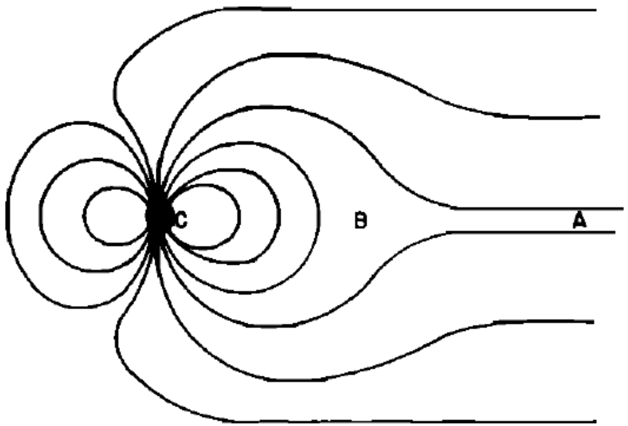

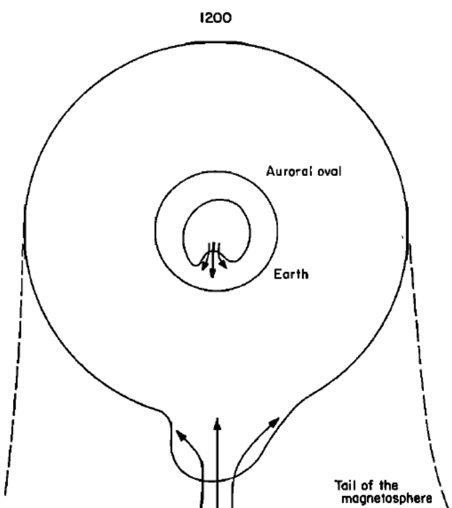

a. The solar wind drags field lines from the region of closed field lines into the tail, either by viscous forces, or by the neutral-point mechanism proposed by *Dungey* [1958]. There is a resulting increase in the tail magnetic field strength and a storing of potential energy.

b. The polar substorm begins when field lines recombine in an implosive fashion at the neutral sheet, in the manner indicated by *Petschek* [1964]. This recombination implies the release of stored potential energy.

c. The recombined flux tubes are added to the night side of the closed region as a giant bulge, causing auroral effects.

d. The flux tubes flow around the closed region toward the day side, causing the magnetic substorm and further auroral effects.

This presentation is being recorded.

Credit to Axford (1965) and Dungey (1966)

McPherron et al., 1973

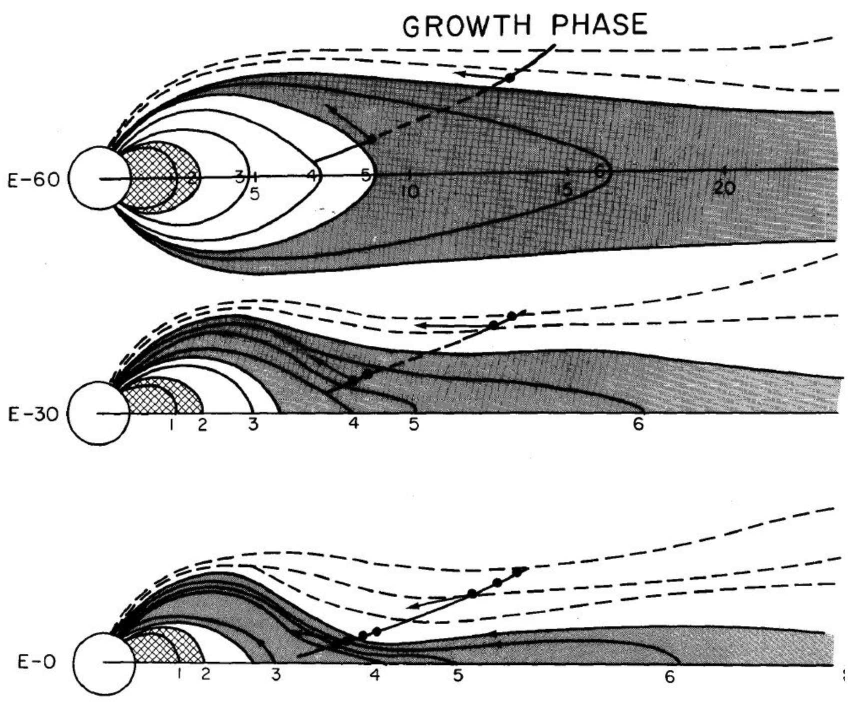

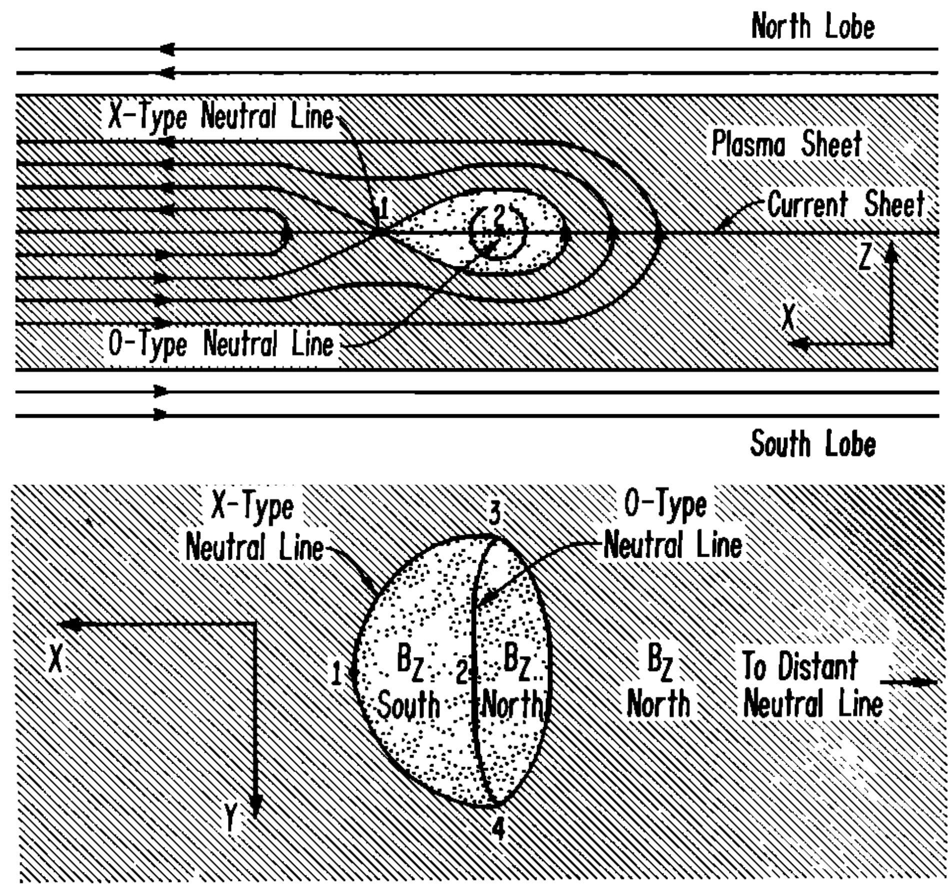

JGR, June 1973

Radio Science, Nov. 1973

This presentation is being recorded.

Substorm current wedge

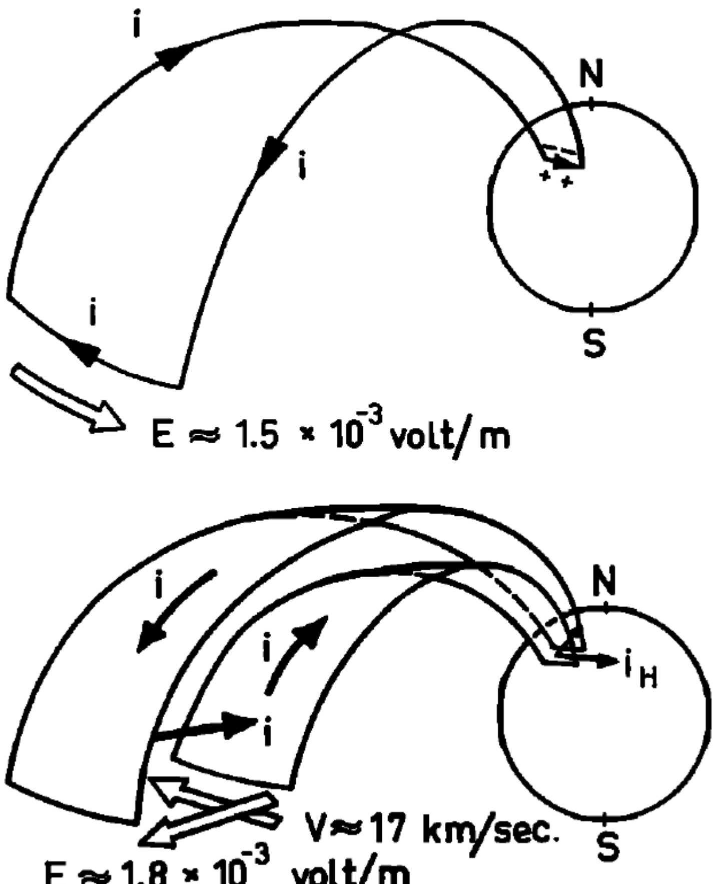

Boström, 1964

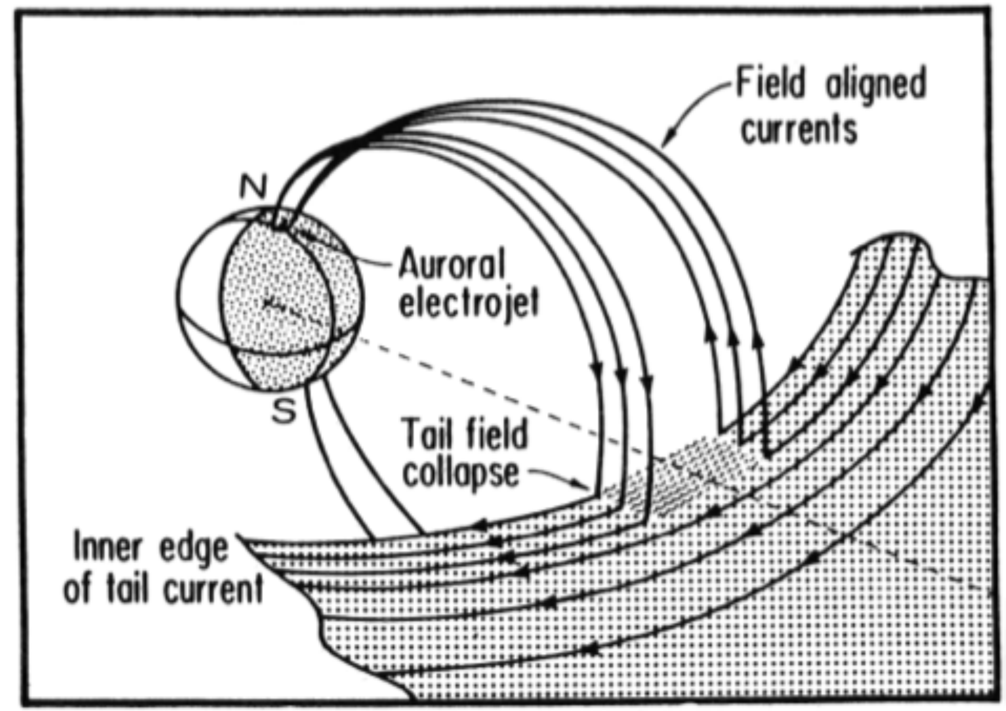

McPherron+, 1973

Theory of substorm mechanism, Schindler 1974

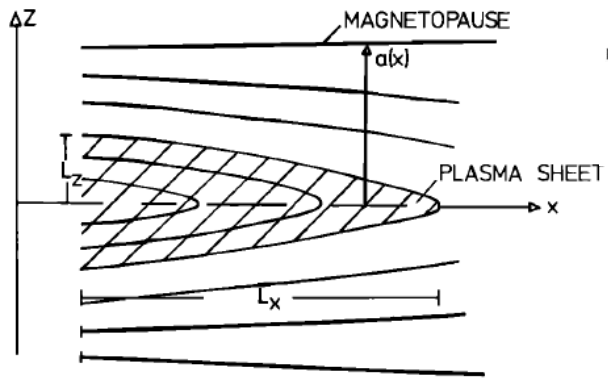

Tail configuration,
finite $B_z > 0$,
destabilization by
reduction of B_z, L_z
Onset of (ion) tearing mode

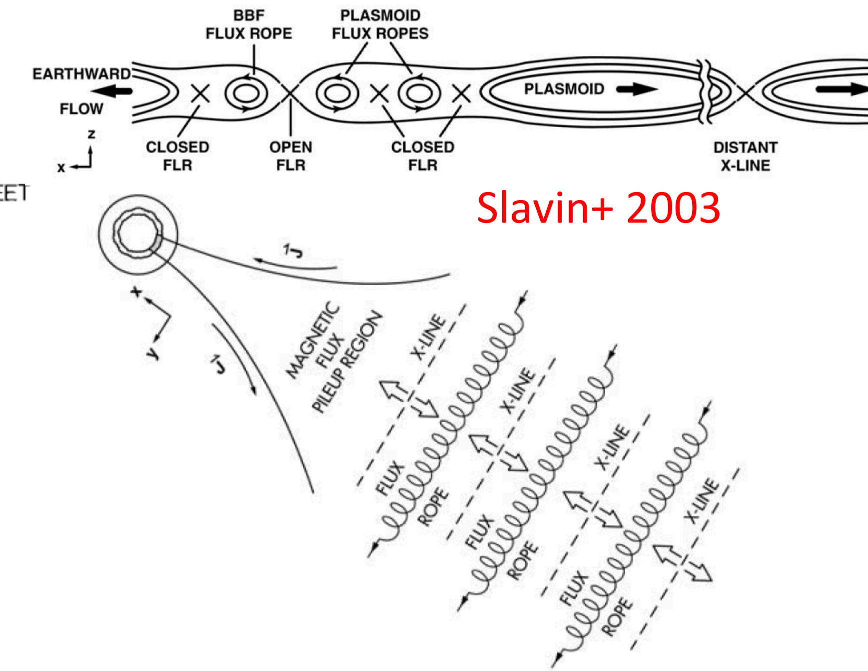

Slavin+ 2003

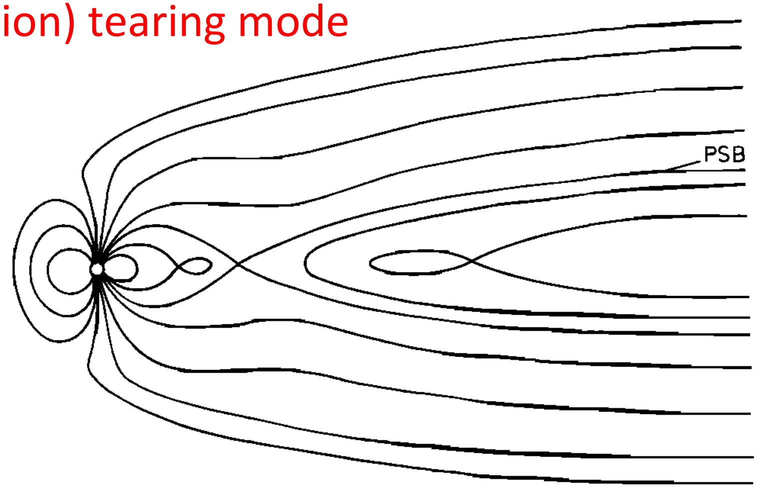

However: Ion tearing stabilized for small B_z
e.g., Pellat+ 1991, Pritchett 1994,
Schindler 2007

Substorm Particle "Injections"

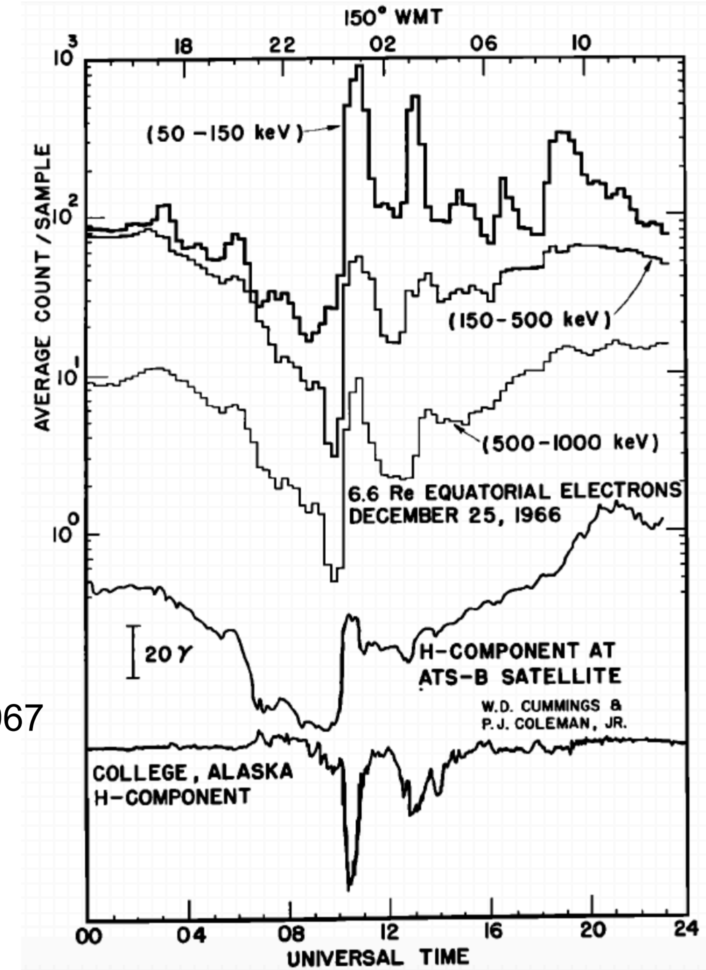

[Parks & Winckler, 1968]

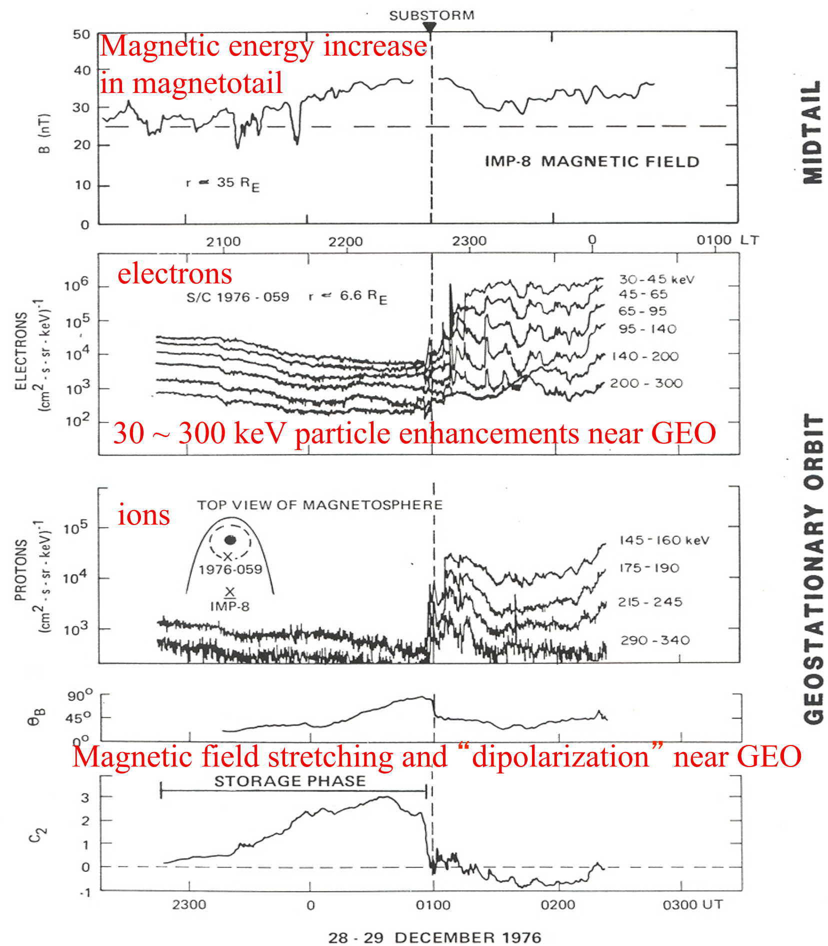

Jelly & Brice, 1967
Konradi, 1967
Lezniak+, 1968
Hones+, 1968
Parks+, 1968

[Baker et al., 1981]

2. Pre-onset: Thin current sheet formation

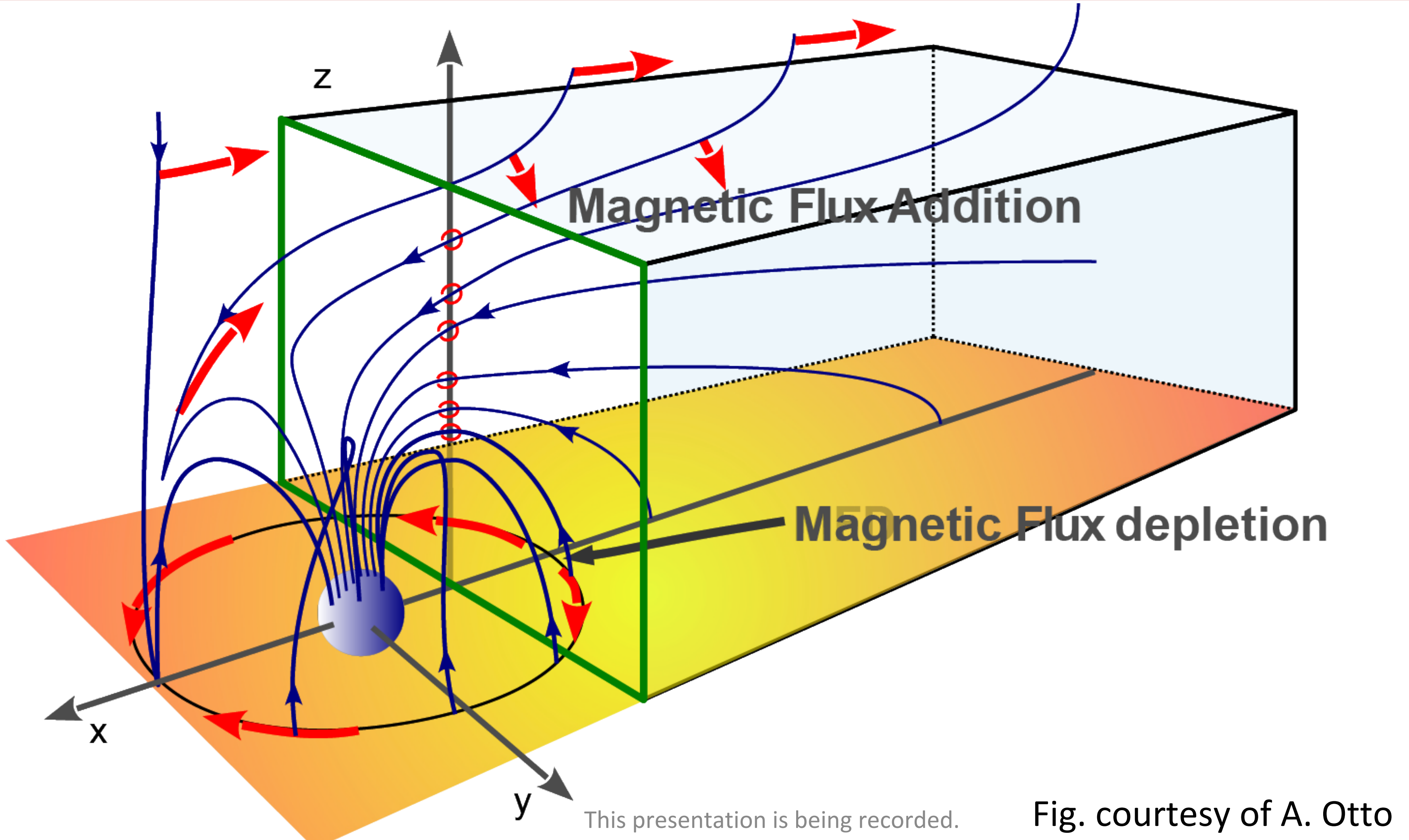

Fig. courtesy of A. Otto

TCS formation: High latitude flux addition

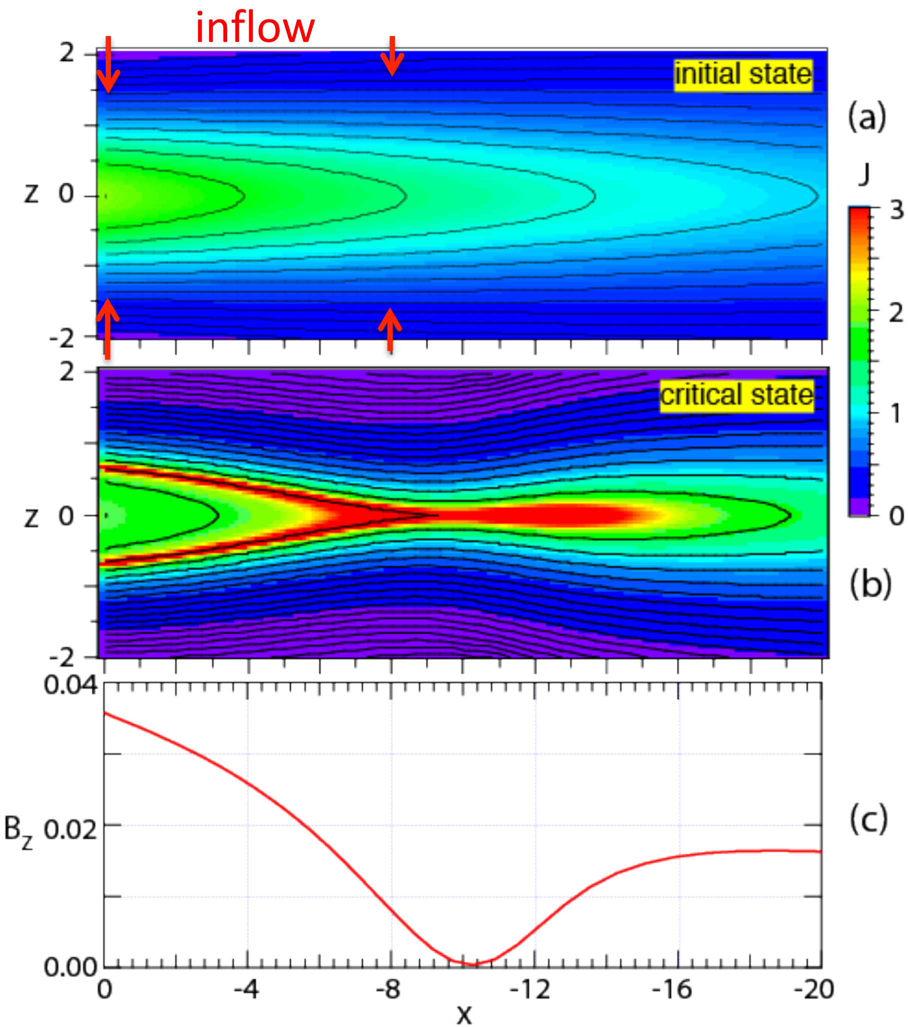

2D Quasi-static theory:
mass & entropy conservation

$$S = \int p^{1/\gamma} ds / B = p^{1/\gamma} V$$

$$V = \int ds / B$$

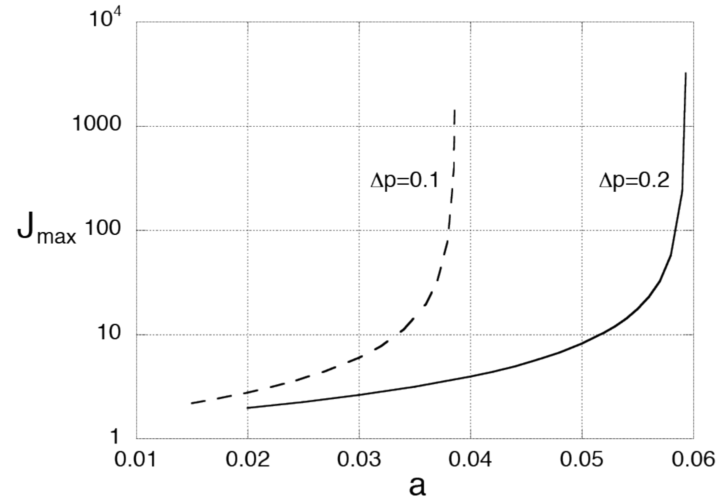

Finite deformation leads to critical point, loss of equilibrium, thin current sheet, Bz minimum

(Birn & Schindler, 2002)

TCS formation: Low latitude flux depletion

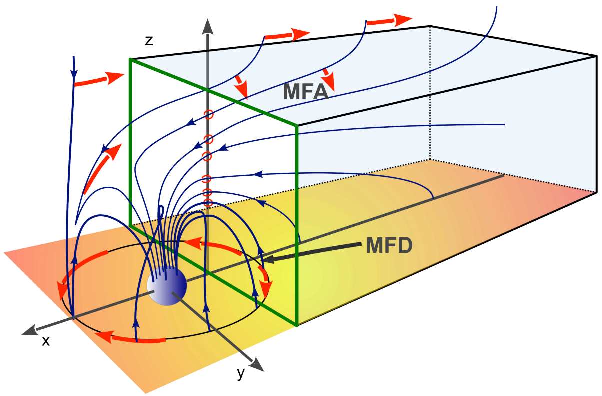

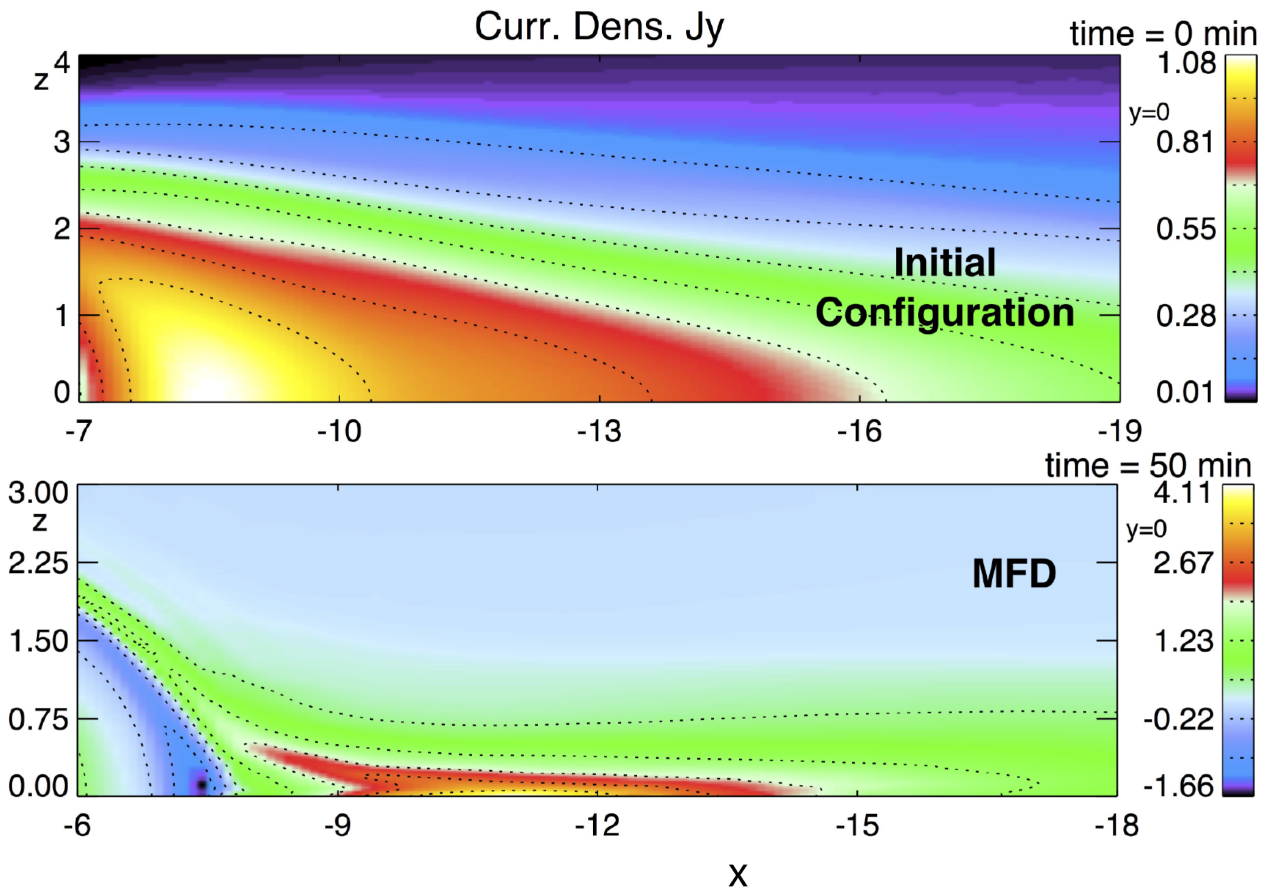

(Hsieh & Otto, 2014, 2015; Otto+, 2015)

TCS formation: Low latitude flux depletion

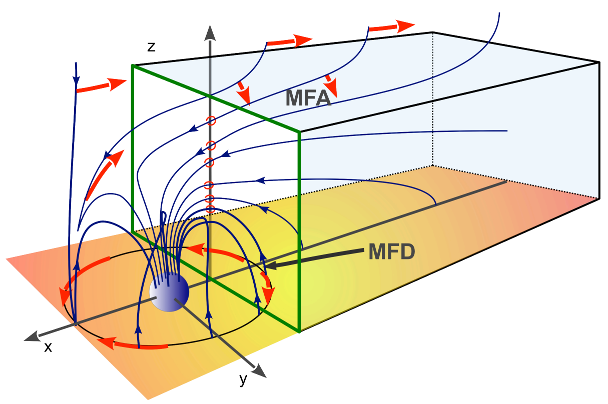

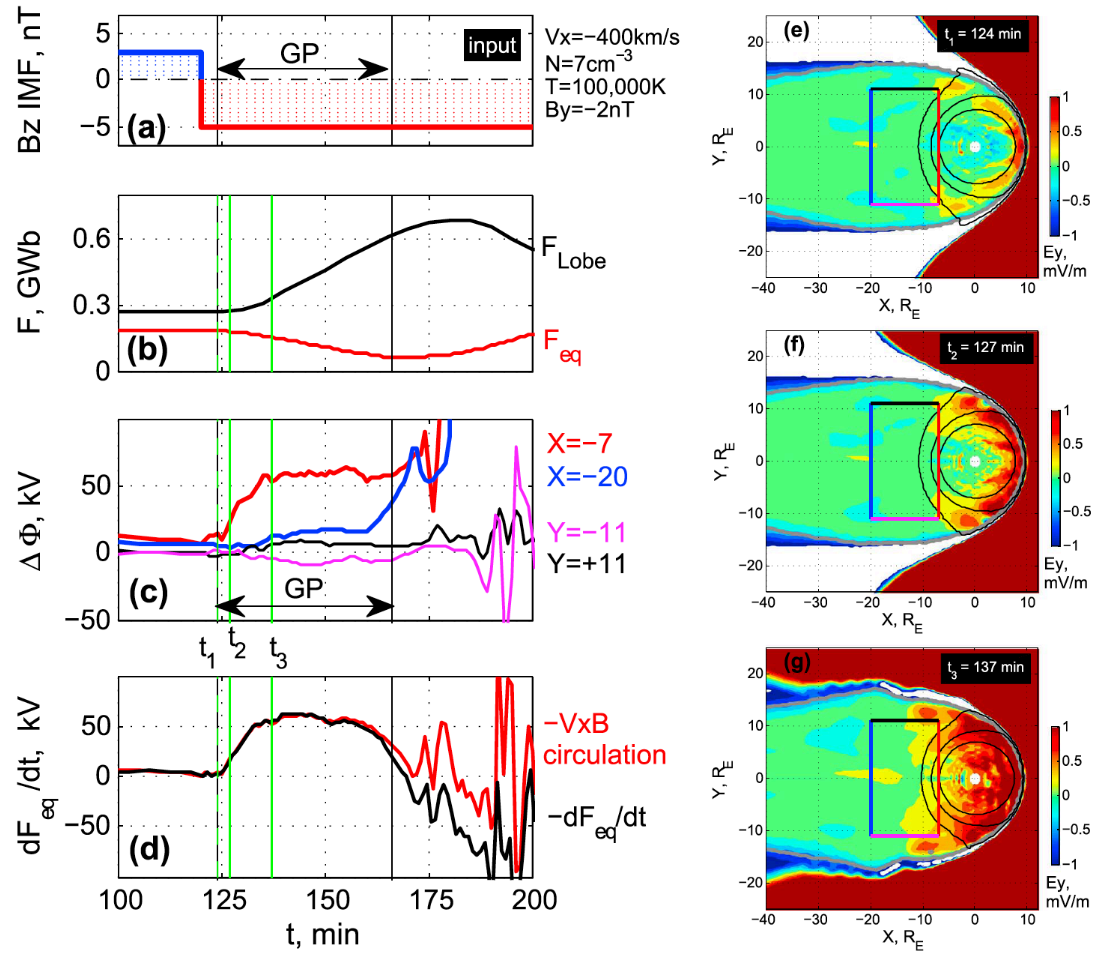

Gordeev+, 2017 (global LFM simulation): Removal of closed magnetic flux by return convection controls the major reconfiguration of near magnetotail during substorm growth phase

3. Onset of Reconnection: PIC Simulations

limited driving m_i/m_e = 100, 2D

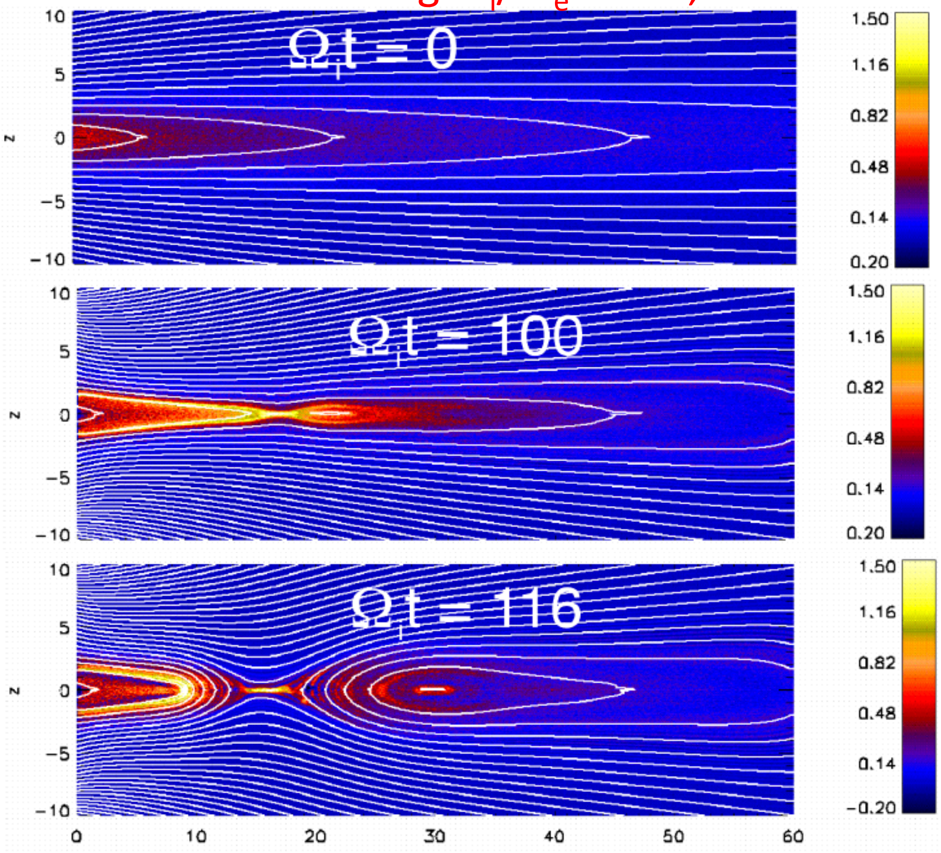

Hesse & Schindler 2001

continued driving m_i/m_e = 100, 3D

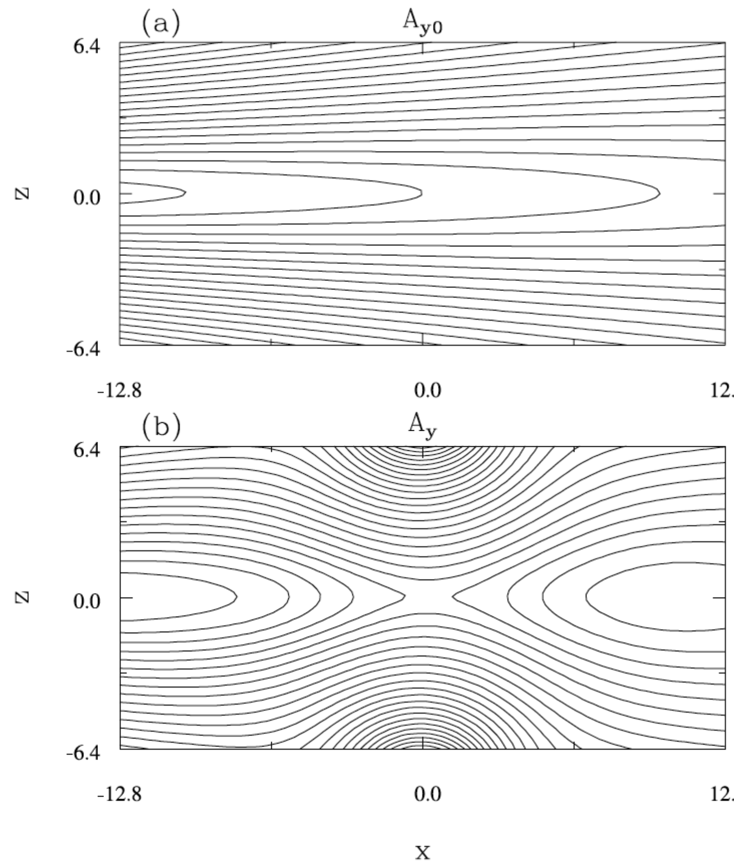

(Pritchett&Coroniti, 1993) Pritchett 2005

Finite deformation of stable tail (LiuYH+ 2014)

Initial state: $L_z = 2\ d_i$, $B_z = 0.05\ B_0$

-> stability to tearing (e.g., Brittnacher et al., 1995; Daughton, 1999)

Monotonic entropy function, $S = P^{1/\gamma}V$

-> stability to ballooning/interchange (e.g., Schindler, 2007)

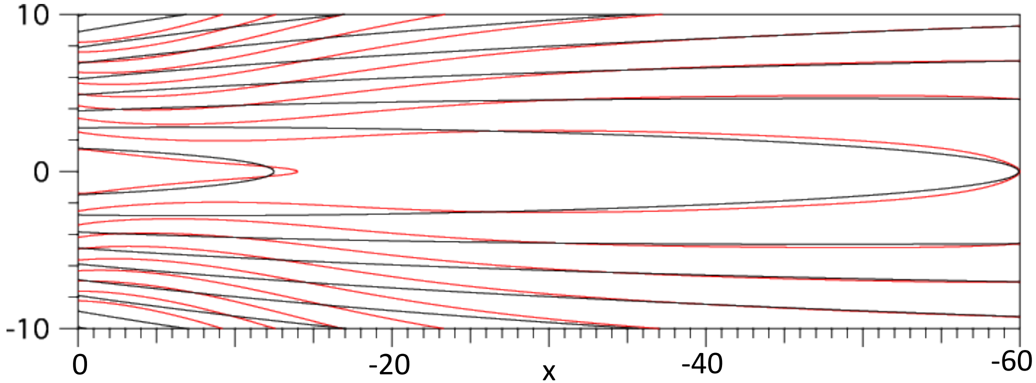

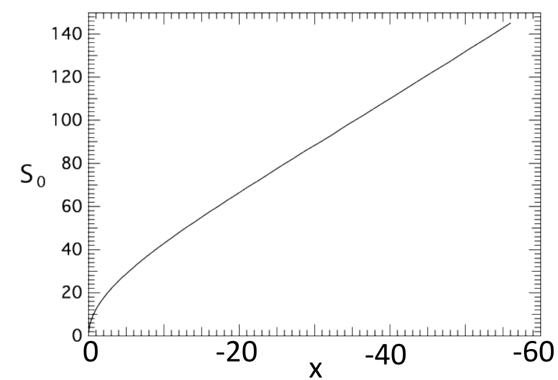

Finite deformation of tail equilibrium by temporally limited external inflow of magnetic flux; (vary amplitude a, m_I/m_e up to 1836)

Formation of thin embedded current sheet – may or may not lead to onset, loss of equilibrium

This presentation is being recorded.

(LiuYH et al., 2014)

Finite deformation (Liu+ 2014)

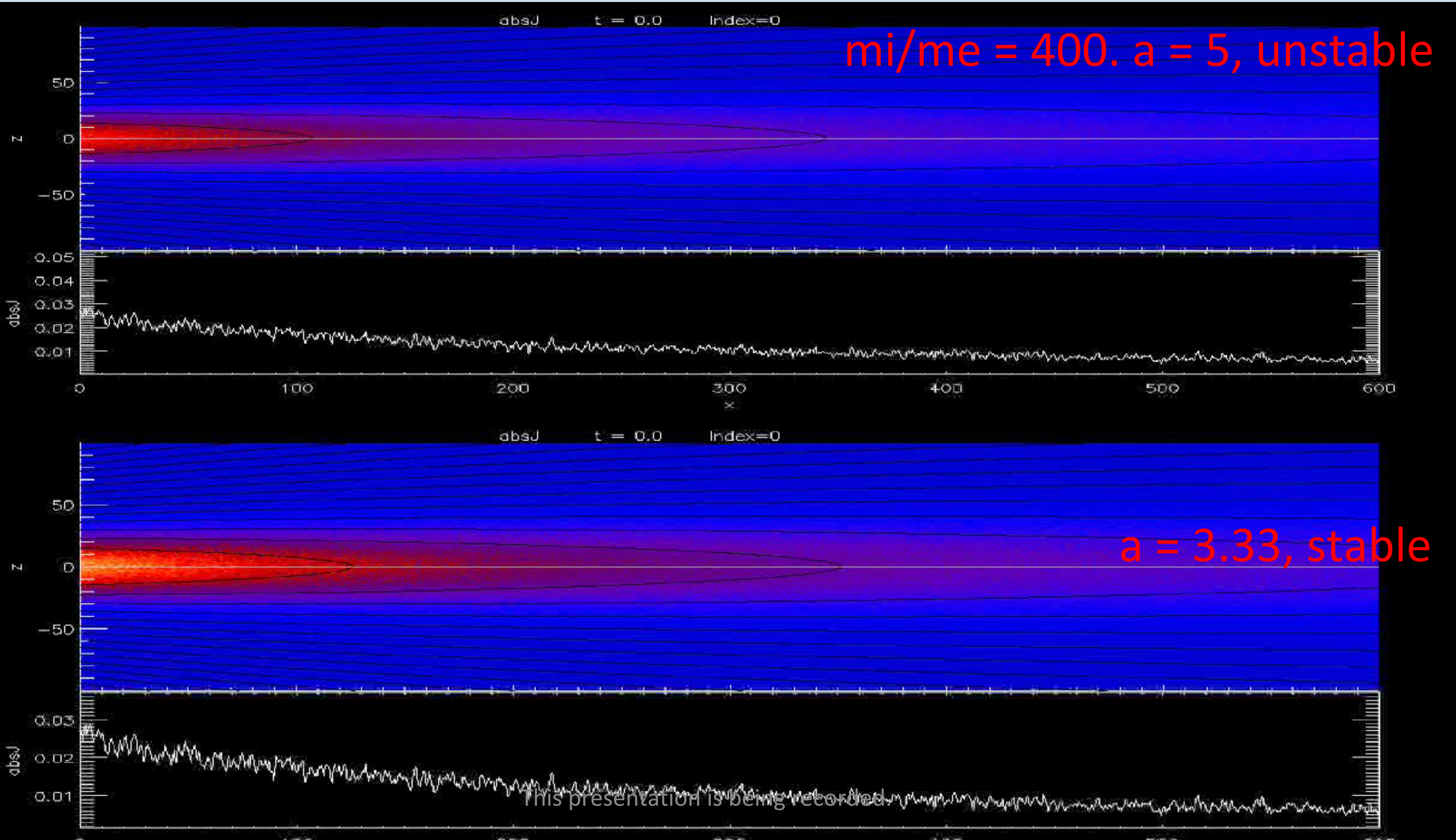

Onset depends on deformation amplitude a

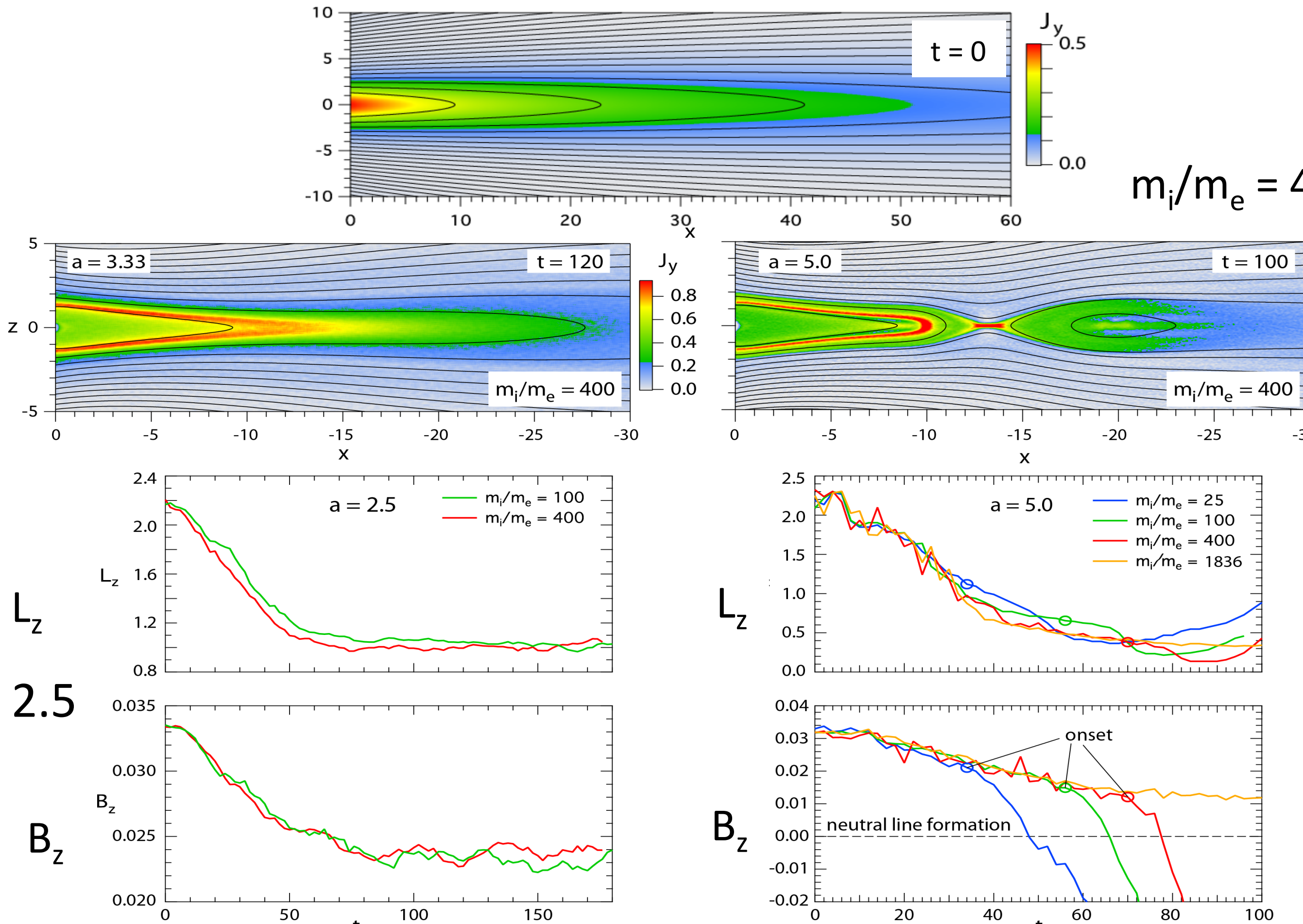

$m_i/m_e = 400$

a = 3.3
stable

a = 5
unstable

L_z

L_z

a = 2.5

a = 5

B_z

B_z

(Liu+ 2014)

Onset & Evolution: Dependence on Mass Ratio

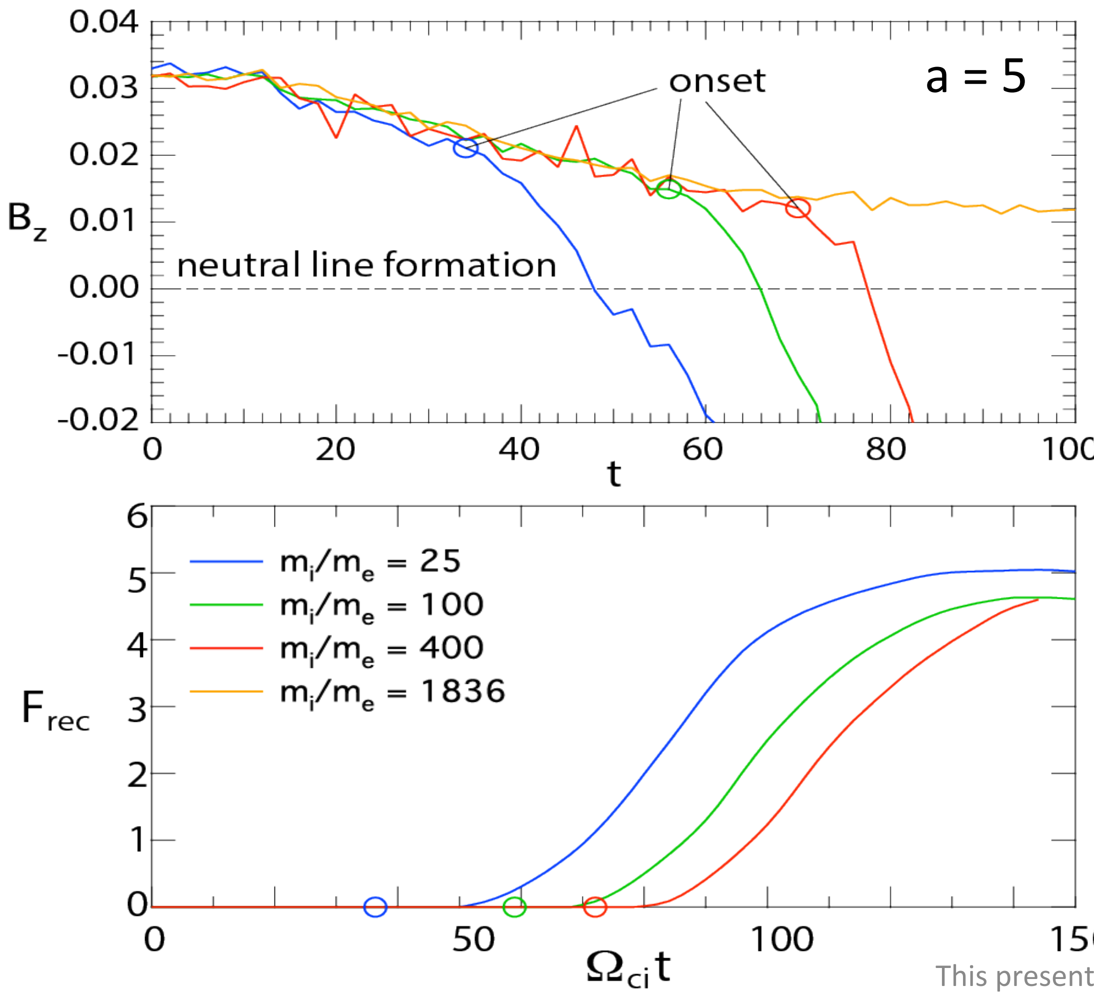

Early evolution independent of m_i/m_e, consistent with MHD

Onset depends on mass ratio

True mass ratio onset requires stronger deformation

Evolution after x-line formation does not depend on mass ratio (consistent with GEM studies)

(Liu+ 2014)

Onset dependence on mass ratio m_i/m_e, L_z, B_z

$$\frac{L_z}{d_i}$$

$$b = \frac{B_z}{B_0}$$

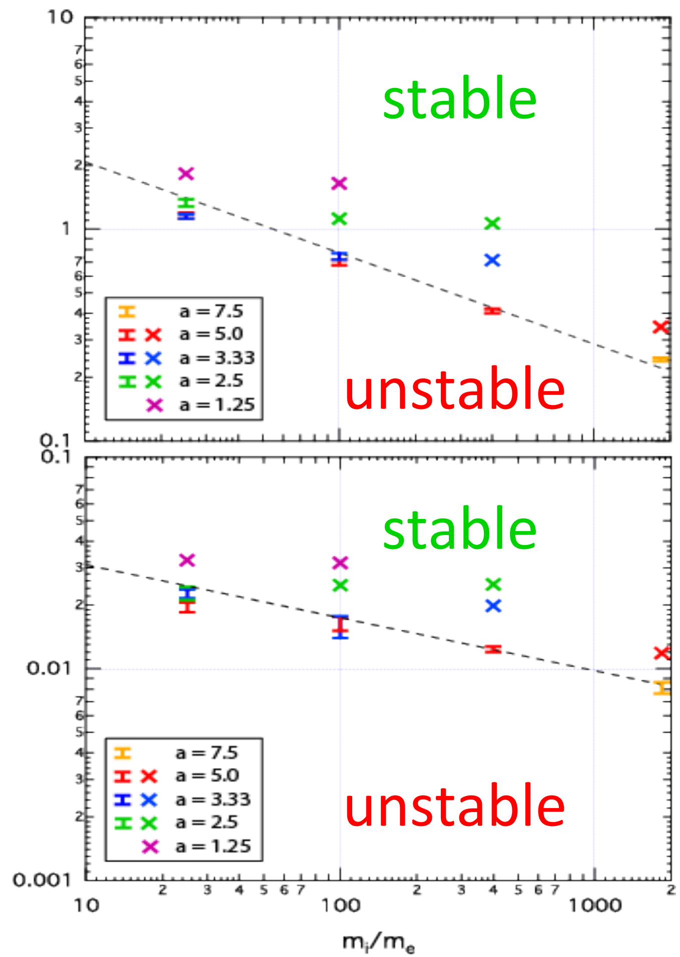

$\sim m_i/m_e^{-0.4}$

$\sim m_i/m_e^{-0.25}$

(Liu+ 2014)

Unstable mode: electron tearing

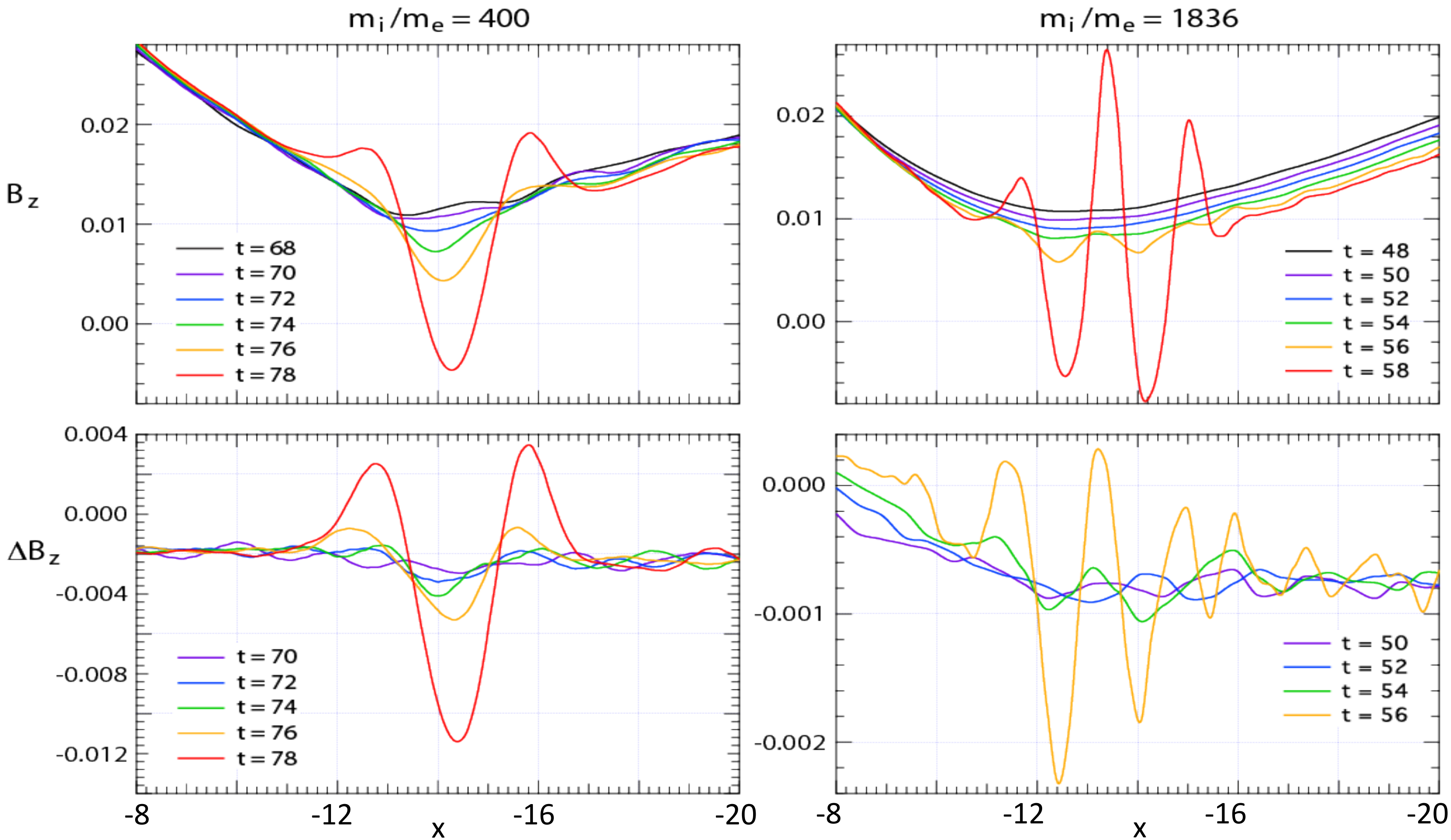

(Liu+ 2014)

Evolution of tail reconnection at m_i/m_e=1836

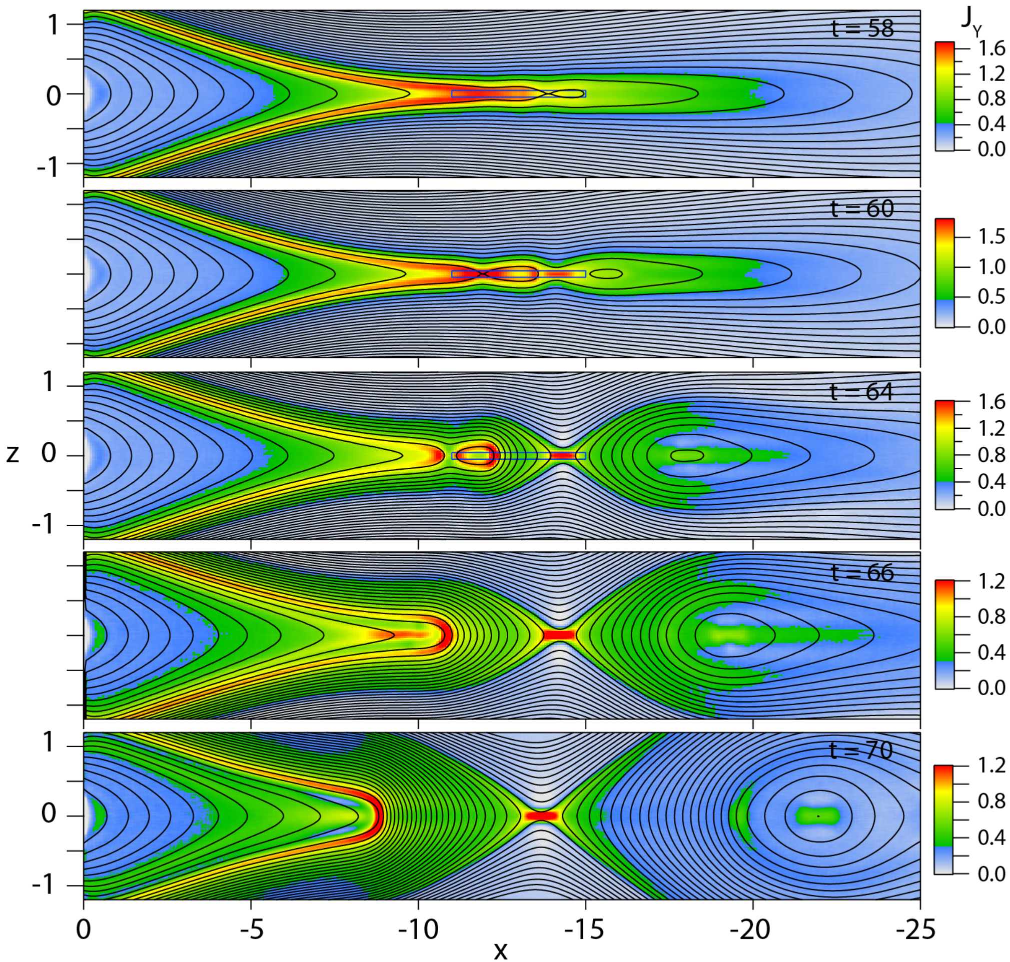

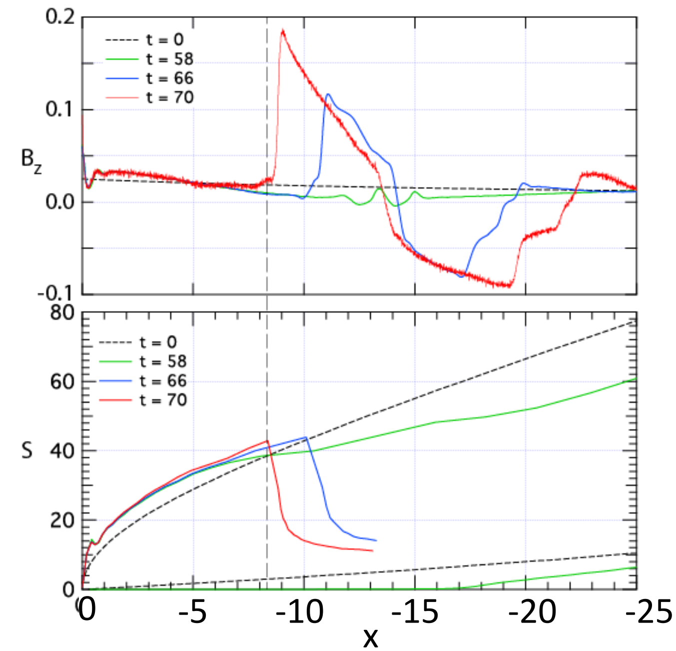

Temporary secondary islands
Steep dipolarization front
Enhanced Bz – reduced entropy, not pile up of external flux

This presentation is being recorded.

(Figs. from Sitnov+2019, data by Daughton, Liu+ 2014)

Summary: Onset & Early Evolution

- CS thinning, onset of tearing instability depend on the amount of deformation, localization (continuous driving not necessary)
- Onset requires both (**local**) thinning and reduction of Bz (go together under external deformation)
- Early, stable evolution independent of mass ratio, consistent with MHD
- Onset of instability depends on mass ratio (electron tearing)
- Unstable tearing mode rises even before Bz changes sign (brief period)
- Fast evolution after x-line formation independent of mass ratio
- PIC (2D) evolution conserves entropy integral prior to onset: ballooning stability before onset of tearing, but plasmoid loss changes entropy integral, may enable ballooning instability

4. Dynamic Evolution: 3D MHD Simulation

2D:
(Leboeuf+, 1978)
Birn, 1980
Scholer&Otto, 1980
Lyon+, 1981
3D:
(Leboeuf+, 1981)
Birn&Hones, 1981
Brecht+, 1982
Ogino+, 1986
Fedder&Lyon, 1987
Walker+, 1988
Ogino+, 1994
Watanabe&Sato, 1990
Fedder+, 1995
Tanaka+, 1995
Lyon+, 1998
Wiltberger+, 2000

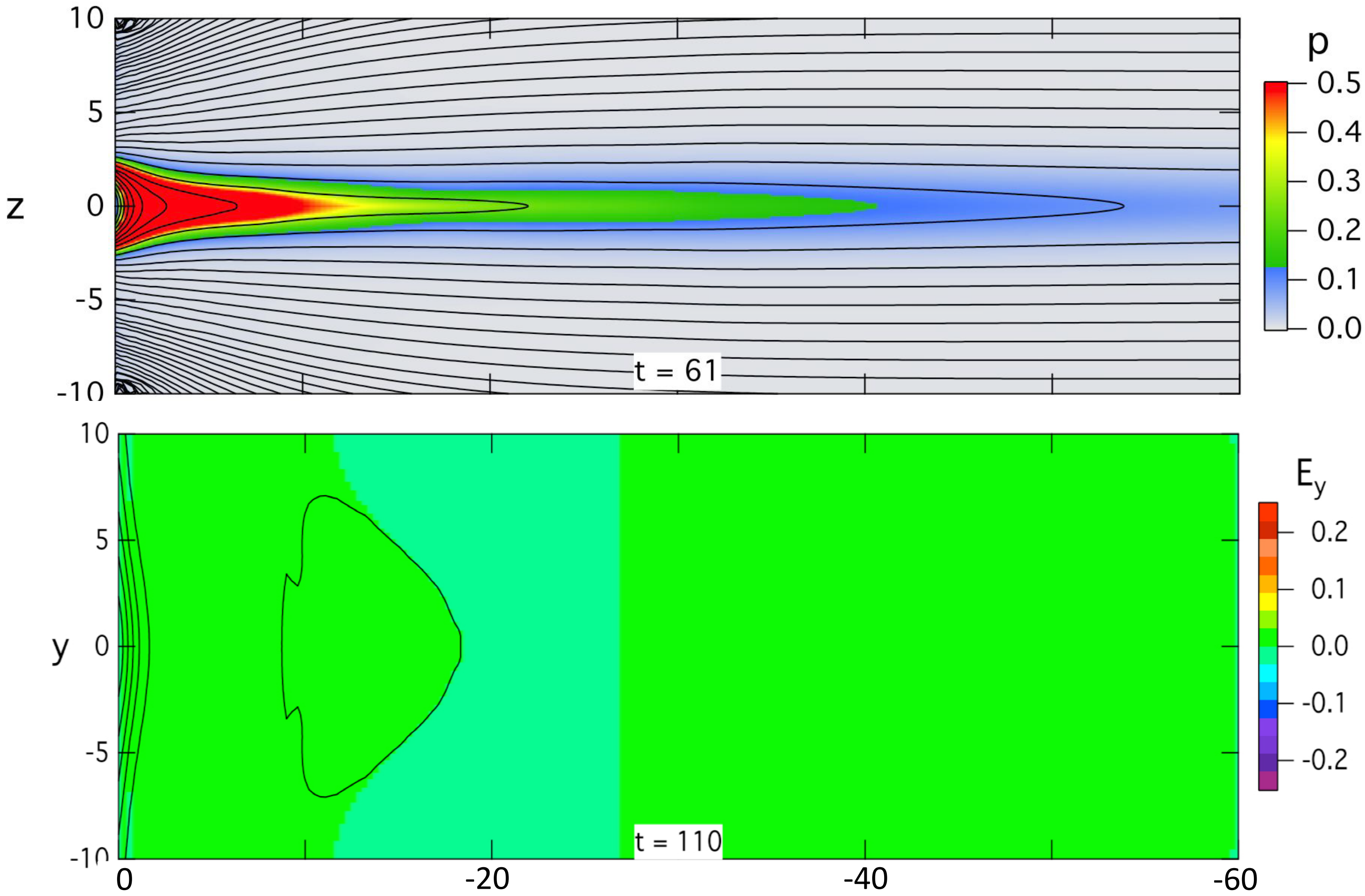

(Birn+ 2011)

Entropy and Flow in 3D MHD Simulation

$$S = \int p^{1/\gamma} ds / B$$

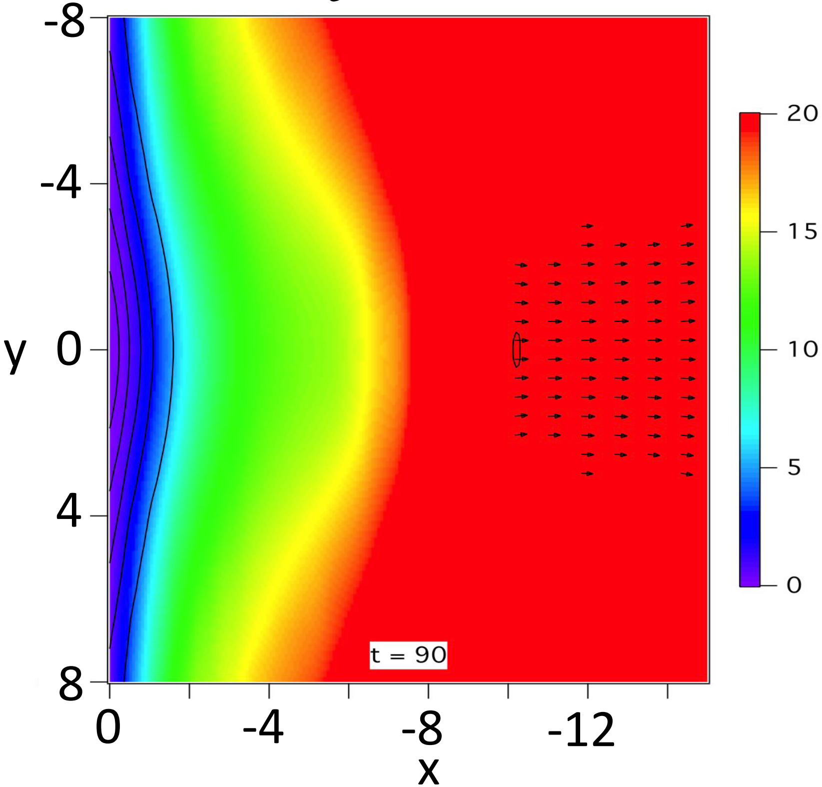

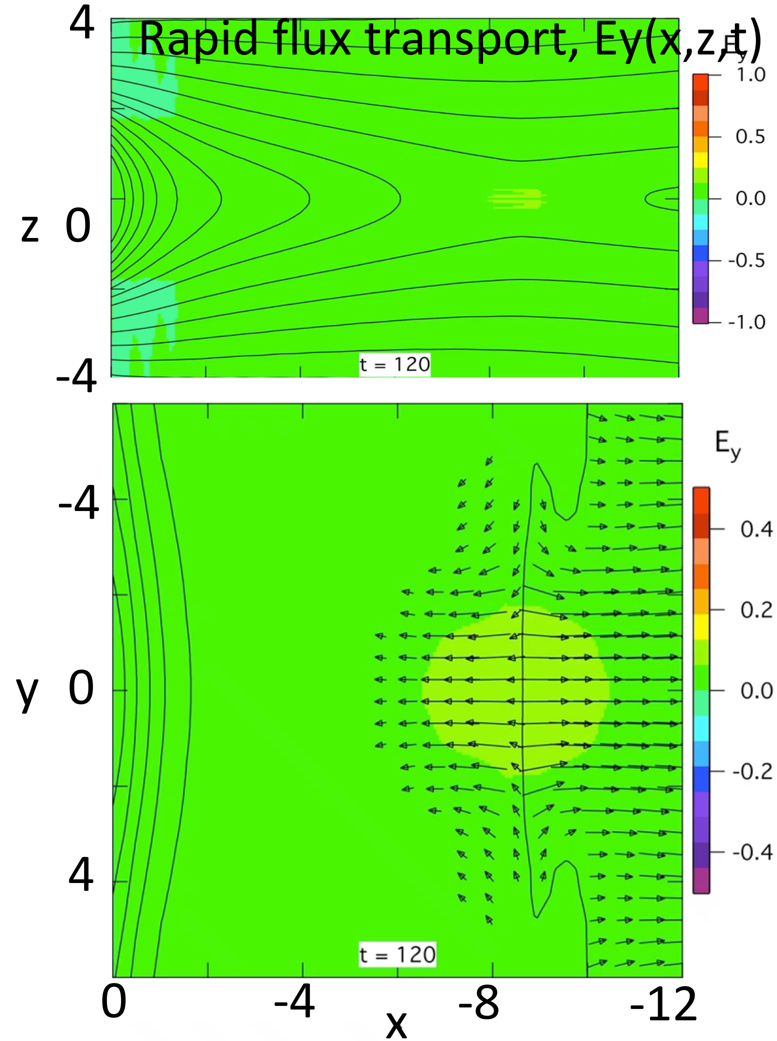

3D MHD Simulations & Observations

THEMIS observations
(Panov et al., 2010)

MHD simulations
(Birn et al., 2011)

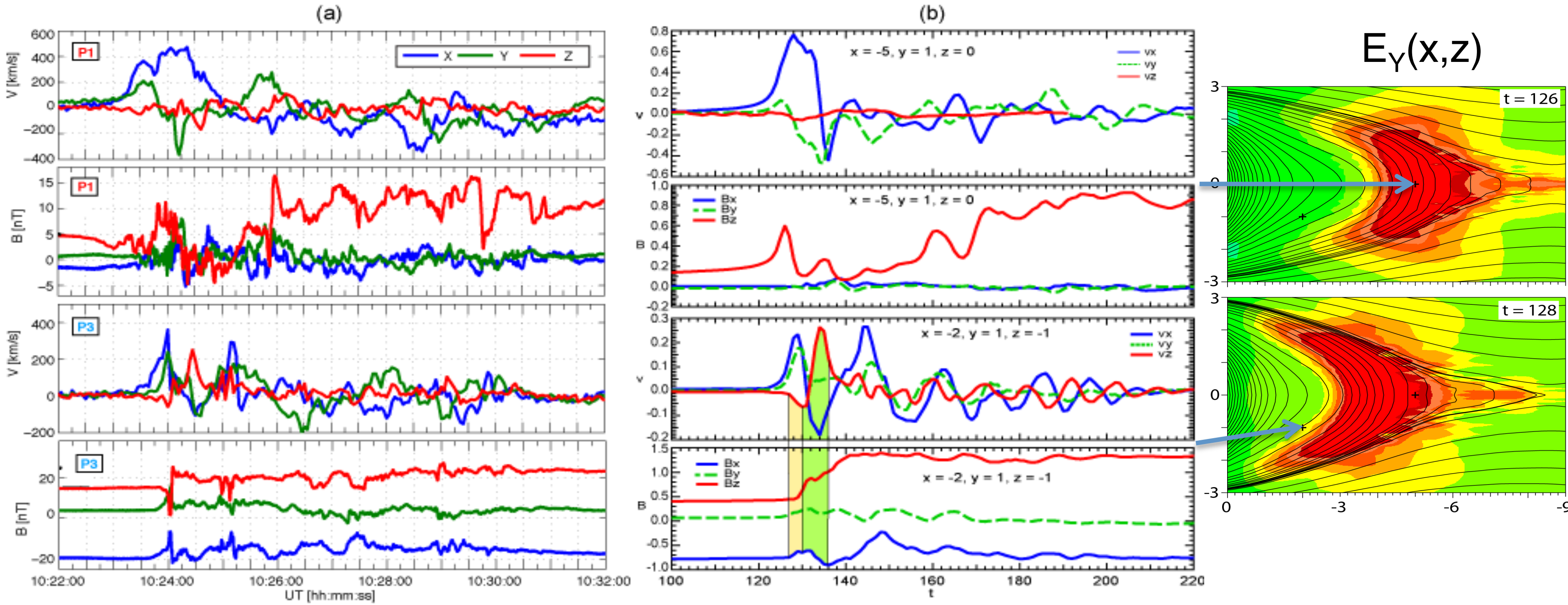

Bouncing, pulsating, dipolarization sequences

This presentation is being recorded.

Buildup of substorm current wedge in MHD

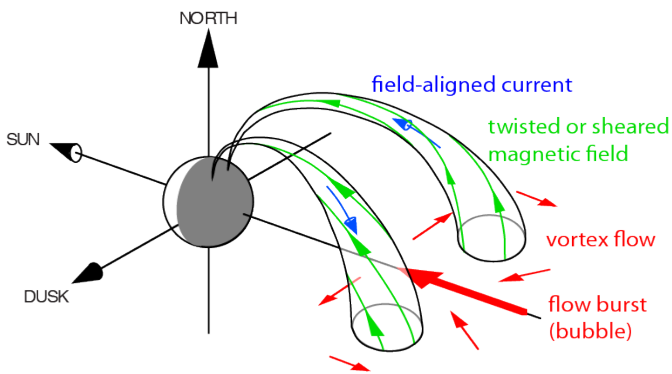

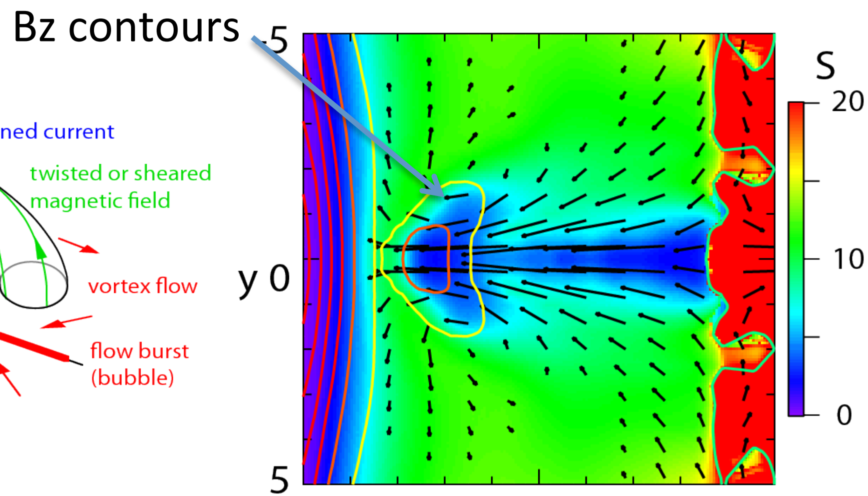

$$\mathbf{j}\times\mathbf{B}\approx\nabla p$$

$$\mathbf{j}_\perp=\frac{\mathbf{B}\times\nabla p}{B^2}$$

$$\nabla\cdot\mathbf{j}_\parallel=\mathbf{B}\cdot\nabla\frac{j_\parallel}{B}=-\nabla\cdot\mathbf{j}_\perp$$

$$\boxed{j_\parallel\approx\frac{\mathbf{B}}{B}\cdot\nabla V\times\nabla p}$$

$$V=\int ds/B$$

Vasyliunas' formula

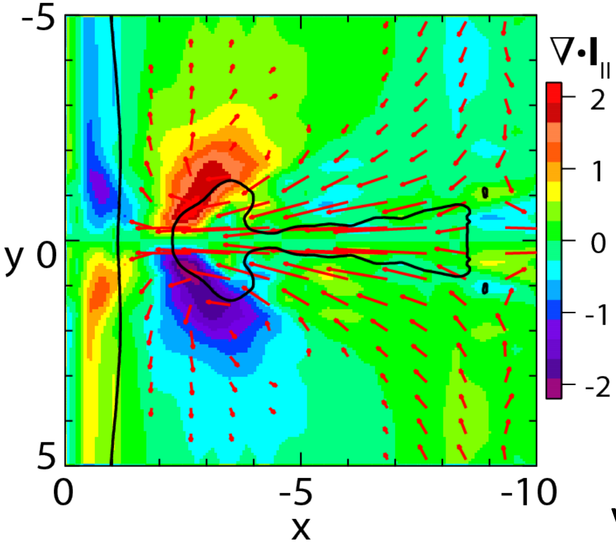

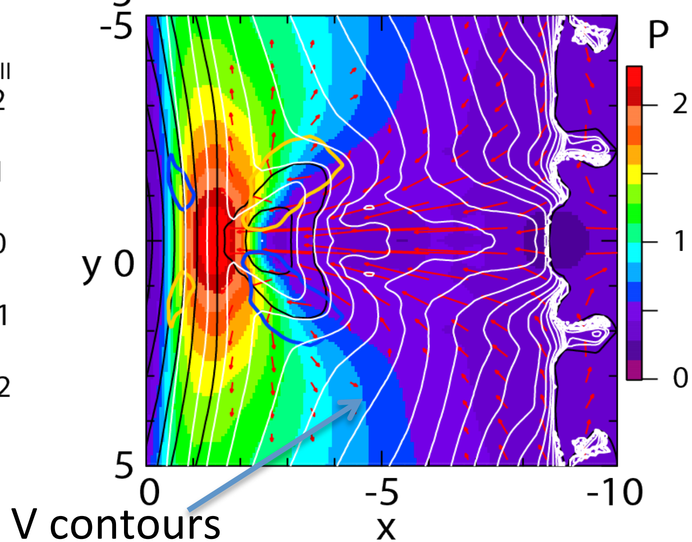

Summary, MHD Results

- Onset of reconnection in near tail leads to fast flow, plasmoid ejection, dipolarization sequence, bouncing, pulsating consistent with observations
- Flow bursts associated with low entropy bubbles, dipolarization
- Individual bursts cause SCW type field-aligned currents
- Multiple bursts can contribute to growth of SCW

5. Particle acceleration in dipolarization events

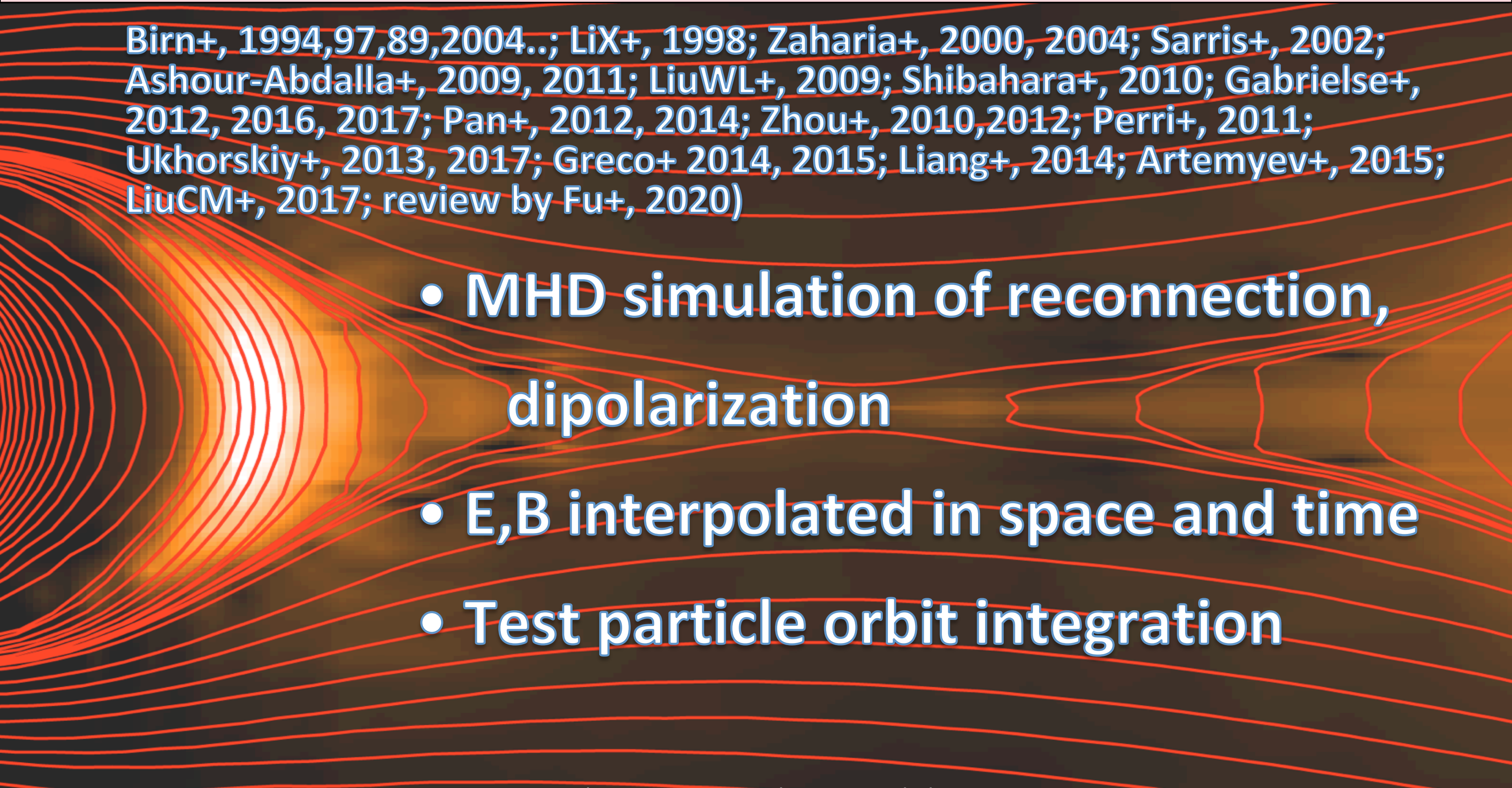

Birn+, 1994,97,89,2004..; LiX+, 1998; Zaharia+, 2000, 2004; Sarris+, 2002; Ashour-Abdalla+, 2009, 2011; LiuWL+, 2009; Shibahara+, 2010; Gabrielse+, 2012, 2016, 2017; Pan+, 2012, 2014; Zhou+, 2010,2012; Perri+, 2011; Ukhorskiy+, 2013, 2017; Greco+ 2014, 2015; Liang+, 2014; Artemyev+, 2015; LiuCM+, 2017; review by Fu+, 2020)

- MHD simulation of reconnection, dipolarization
- E,B interpolated in space and time
- Test particle orbit integration

Test particle tracing in MHD fields

Using time-dependent MHD fields, interpolated in space and time
(cubic spline in space; monotonicity conserving algorithm; avoid spurious $E_{||}$)

Backward tracing from final destination to origin at boundary or initial state

Impose f at origin = f at final location (Liouville mapping)

Reflection at near-Earth boundary accounts for delay from mirroring closer to Earth, based on estimates from orbits in Tsyganenko field model.

Full equation of motion in strongly varying or weak fields (always for ions)

$$\frac{dm\mathbf{u}}{dt} = q(\mathbf{E} + \mathbf{u} \times \mathbf{B})$$

Gyrocenter drift in weakly varying fields (μ_{rel} conserved)

$$\mathbf{v}_\perp = \mathbf{v}_E + \mathbf{v}_{\nabla B} + \mathbf{v}_C = \frac{\mathbf{E} \times \mathbf{B}}{B^2} + \frac{\mu}{q}\frac{\mathbf{B} \times \nabla B}{B^2} + \frac{mv_\parallel^2}{q}\frac{\mathbf{B}}{B^2} \times (\mathbf{b} \bullet \nabla \mathbf{b})$$

$$\frac{dmv_\parallel}{dt} = qE_\parallel - \mu \mathbf{b} \bullet \nabla B + mv_\parallel(\mathbf{v}_E + \mathbf{v}_{\nabla B}) \bullet (\mathbf{b} \bullet \nabla \mathbf{b}) \qquad \mathbf{b} = \frac{\mathbf{B}}{B}$$

$$m = \gamma m_0 \qquad \mu = \frac{\mu_{rel}}{\gamma} \qquad \mu_{rel} = \frac{p_\perp^2}{2m_0 B} \qquad \gamma = \frac{1}{\sqrt{1 - (v/c)^2}}$$

Transition based on adiabaticity parameter ($\kappa^2 = r_{curv}/a_{gyr}$)

Ion acceleration, central plasma sheet

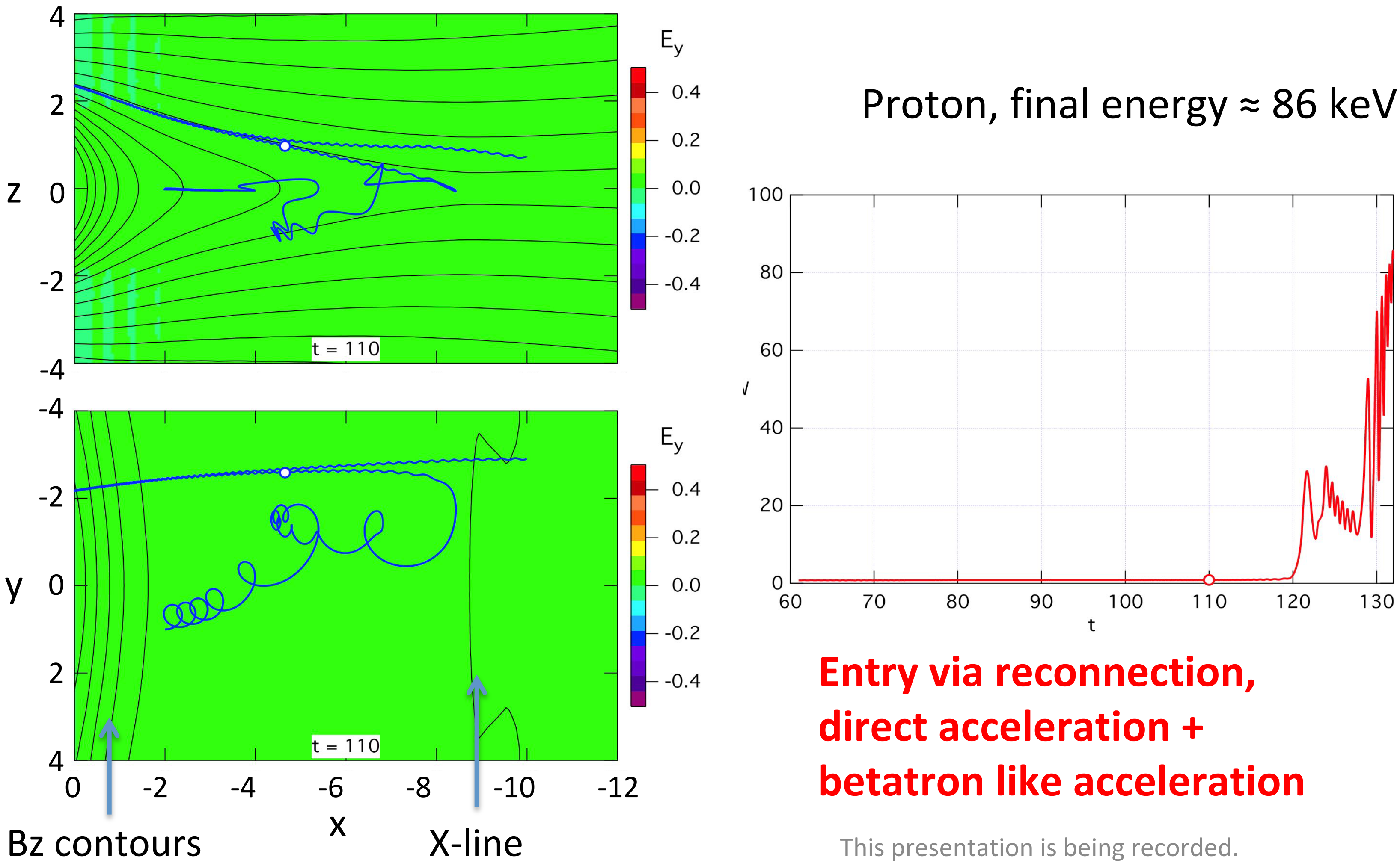

Entry via reconnection, direct acceleration + betatron like acceleration

Ion acceleration, plasma sheet boundary

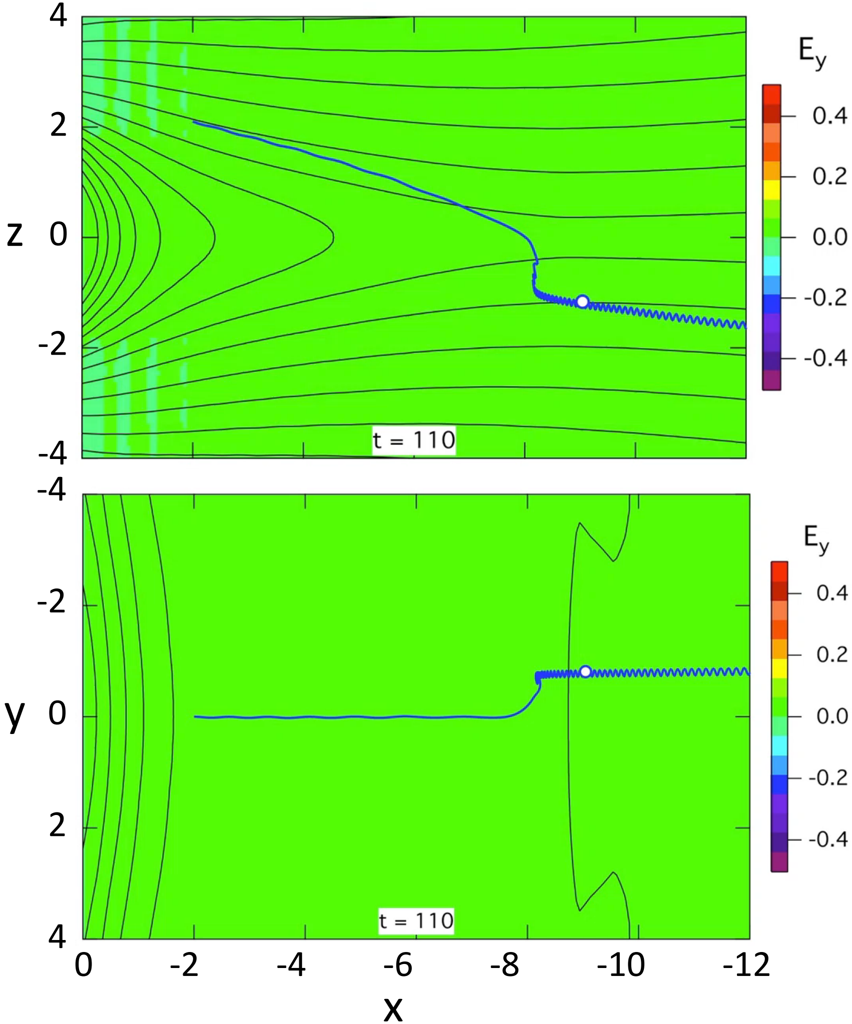

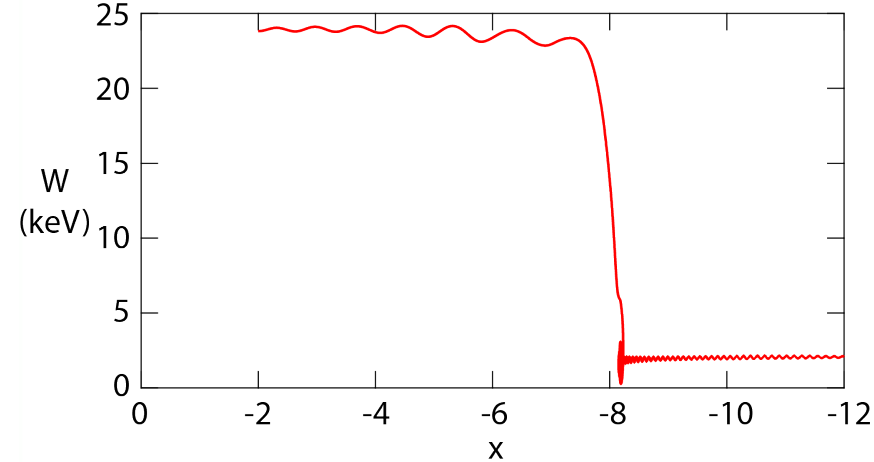

direct acceleration near x-line,
ejection into PSBL beam

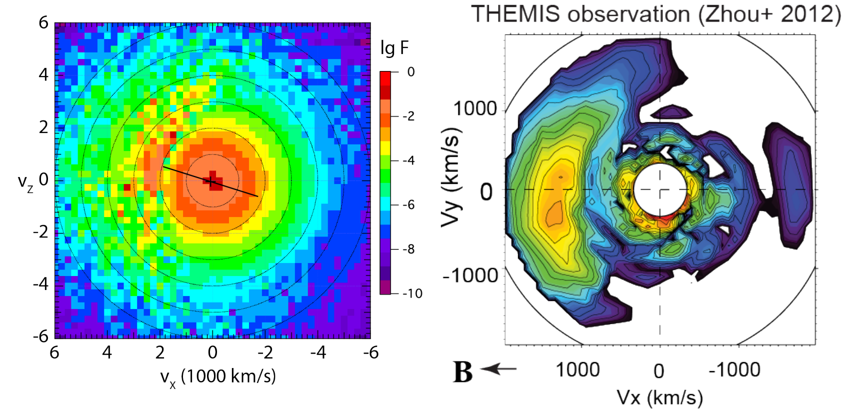

Ion acceleration, PSBL beam

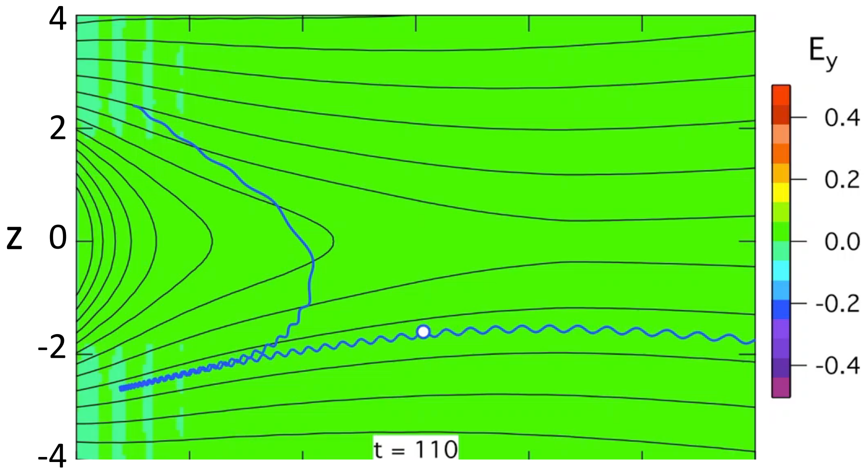

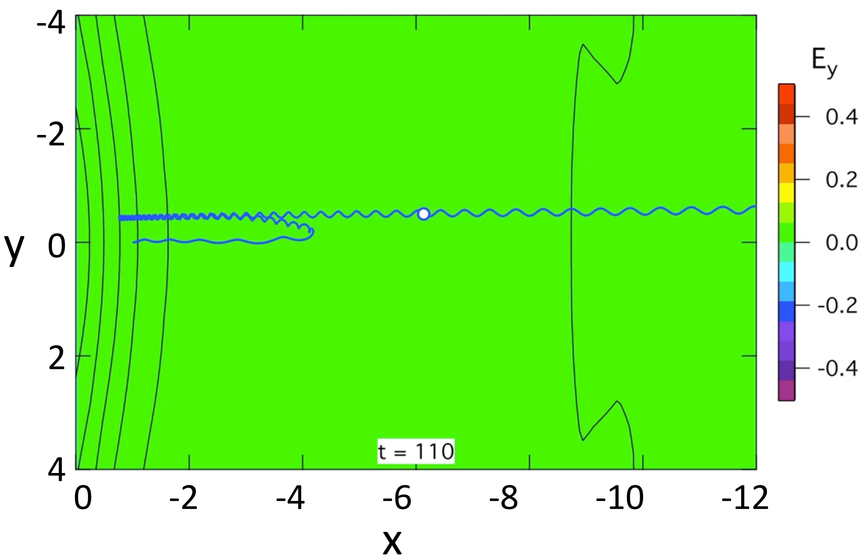

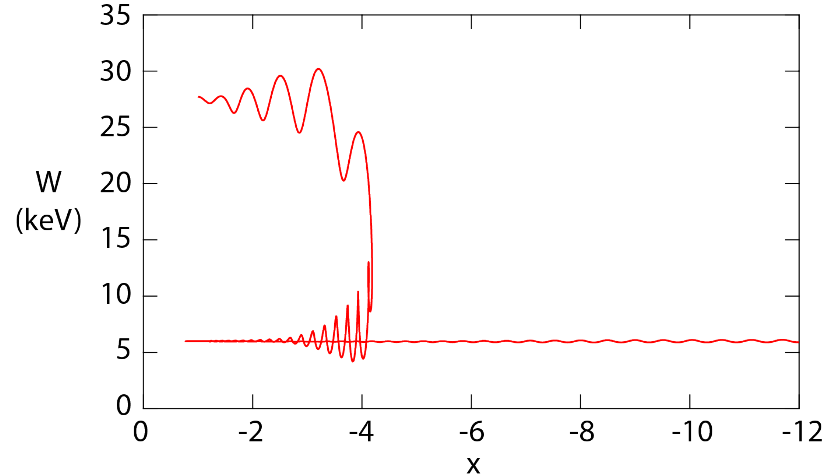

current sheet acceleration (Lyons&Speiser, 1982)
convection surge mechanism
(Quinn&Southwood, 1982; Mauk, 1986)

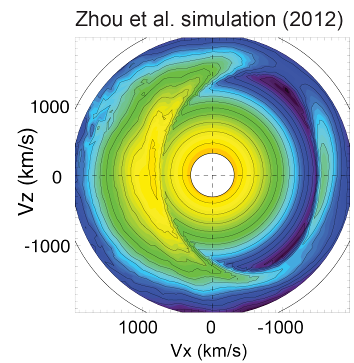

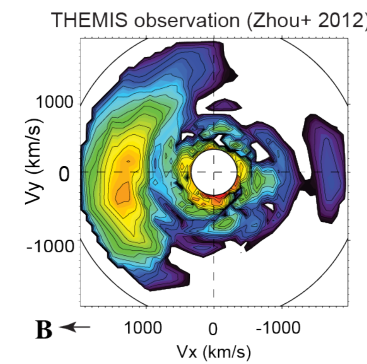

Sample electron acceleration, 90º pitch angle

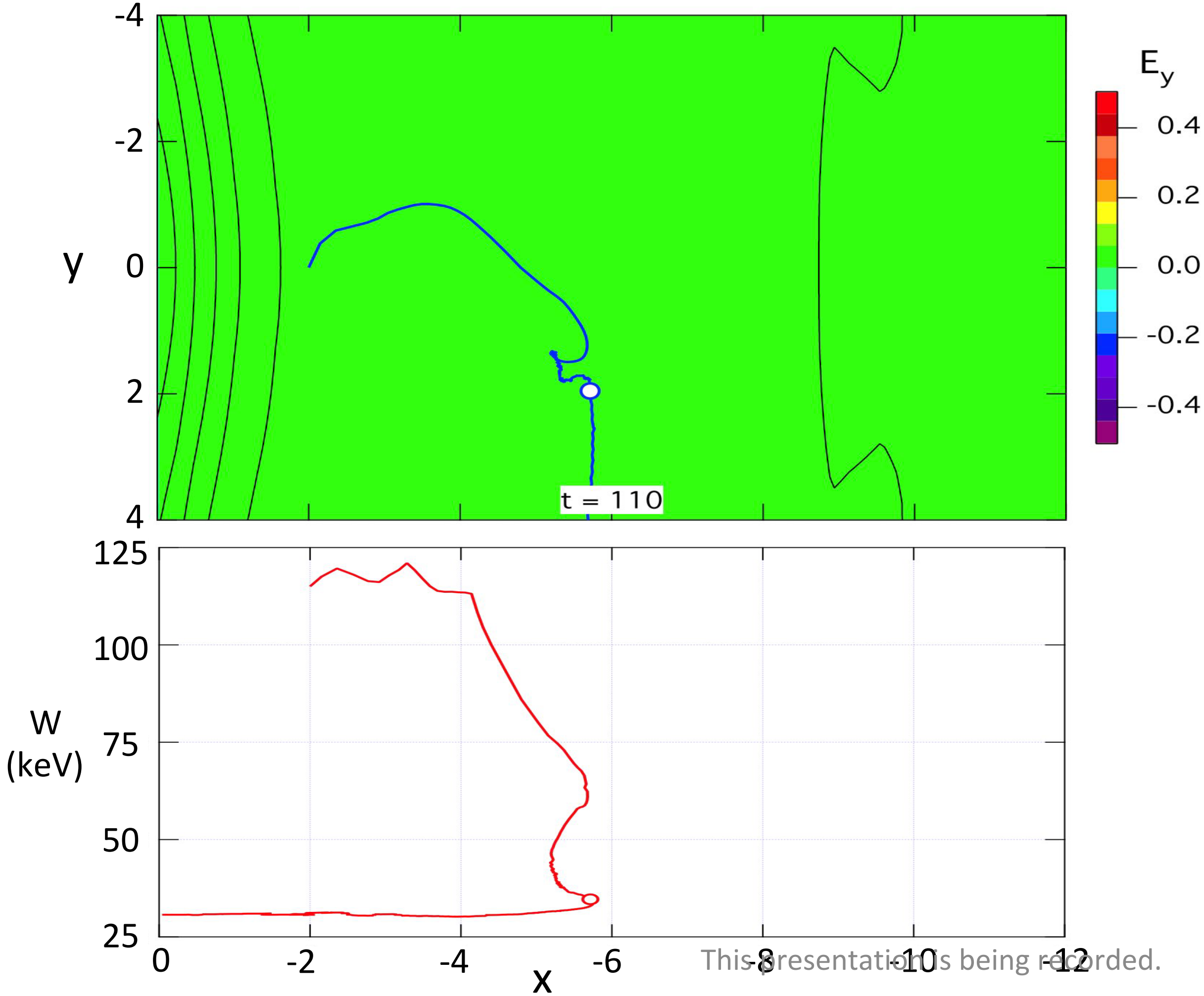

Electron drift path, final energy ≈ 120 keV

Entry via cross-tail VB drift, betatron acceleration

Electron Fermi acceleration (small pitch angle)

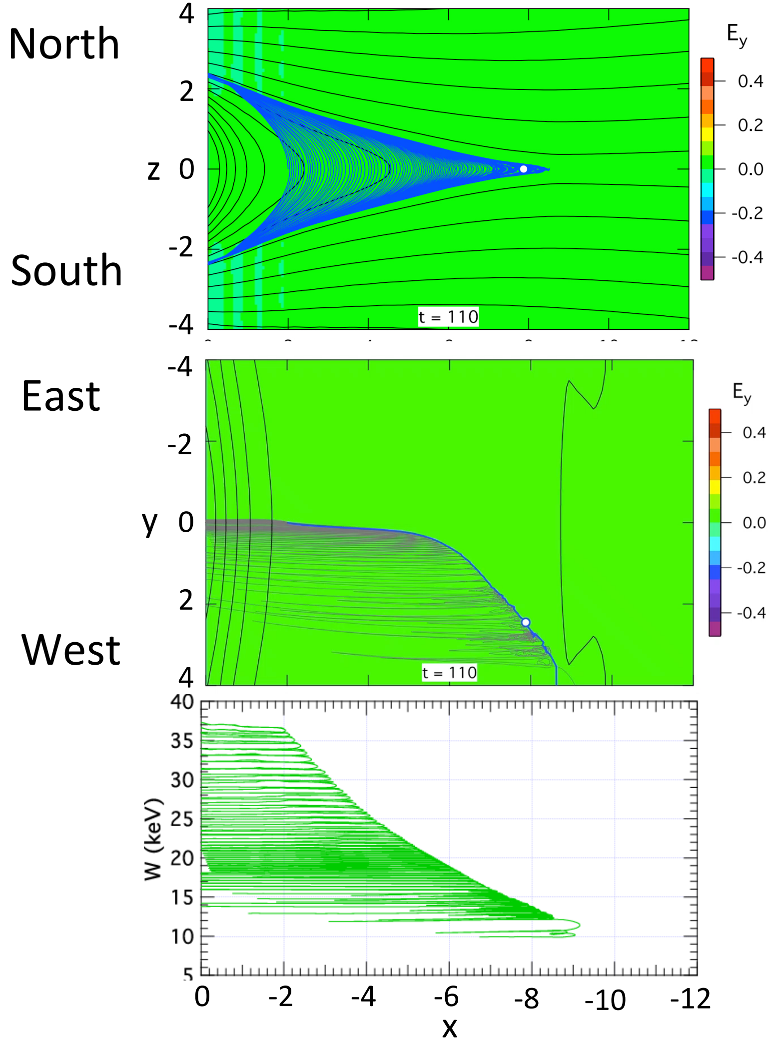

Entry by reconnection or cross-tail drift, earthward E × B drift + cross-tail curvature drift

Repeated energy gain at equatorial crossings between mirroring (1st order Fermi, type B; Northrop 1963; contracting field line, type A)

current sheet acceleration (Lyons&Speiser, 1982)
convection surge mechanism
(Quinn&Southwood, 1982; Mauk, 1986)

This presentation is being recorded.

Electron acceleration

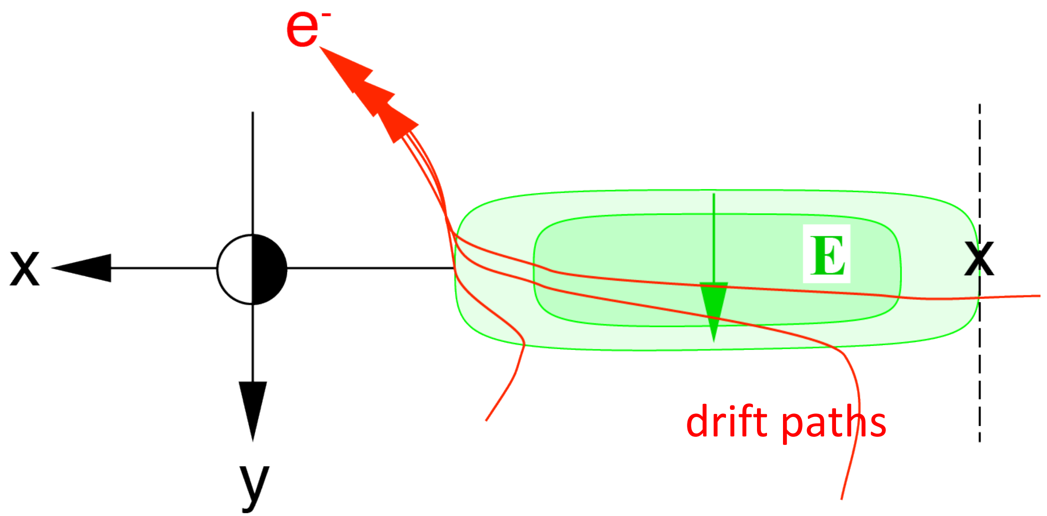

High energy: cross-tail drift > ExB drift

inner plasma sheet source, drift entry

Low energy: ExB drift > cross-tail drift

entry through reconnection from outer plasma sheet

Betatron acceleration: $\mathbf{E}\times\mathbf{B}$ drift toward ∇B $\equiv$ ∇B drift toward -$\mathbf{E}$

Fermi acceleration: $\mathbf{E}\times\mathbf{B}$ drift toward curvature vector $\equiv$ curvature drift toward -$\mathbf{E}$

Summary: Particle Acceleration

Acceleration mainly from field collapse, governed by $E_y = -v_x \times B_z$

- Importance of localization in y
- Betatron acceleration (similar if nonadiabatic)
- 1st order Fermi, type B (or A; current sheet acceleration)

Direct acceleration near x-line or DF generates ion beams near PSBL

Two source regions (comparable importance in magnetotail):

- flanks, inner tail	- drift entry	- early, higher energy
- outer plasma sheet/PSBL	- reconnection entry	- later, lower energy

Explains drop at lower energies, increase at higher energies

Acceleration limited by $\int E_y \, dy$ (few 100 keV)

Summary: Answers & Open Questions

Growth phase, thin current sheet formation: Local, from lobe flux addition or CPS depletion

- What is the relative importance of flux addition vs. depletion?
- What determines where TCSs form?

Onset: Localized current sheet thinning enables onset of tearing, fast reconnection

- What are the actual conditions? In 3D, and with guide field?
- Does turbulence play a role?
- Is there a preceding instability?
- External or internal trigger?

Expansion phase: Shear flows generate FACs, localized Ey is an effective accelerator

- What is the relative role of multiple flow bursts at same location or different locations?
- What is the role of waves? Anisotropy?
- What is the relevance of injections for the ring current?

Recovery phase:

- What stops reconnection?
- How does a neutral line retreat?
- How does the plasma sheet refill?

How do tail features connect to auroral features?